

DESIGN AND FABRICATION OF A
MONOCHROMATOR DRUM/HOUSE FOR A
TWO-AXIS NEUTRON SPECTROMETER

BY

MD. ABDUL HYE CHOWDHURY

Submitted in Partial Fulfilment
of the Requirements for the
Degree of M.Phil.

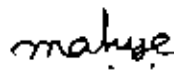


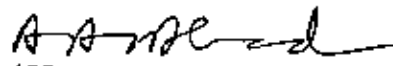
Department of Physics
Bangladesh University of Engineering and Technology
1991

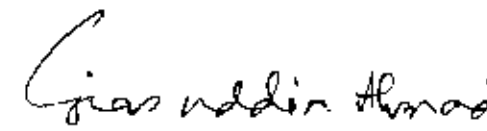


CERTIFICATE

This is to certify that the author is solely responsible for the work reported in this thesis and that this work has not been submitted to any university or elsewhere for the award of a degree/diploma.


(MD. ABDUL HYE CHOWDHURY)
Candidate


(DR. A.A. ZIAUDDIN AHMAD)
Co-Supervisor
Chairman, SPARRO
Agargaon, Dhaka


(DR. GIASUDDIN AHMAD)
Supervisor
Head and Professor
Physics Department
BUET, Dhaka-1000.

ACKNOWLEDGEMENT

The author expresses his sincerest gratitude and gratefulness to his supervisors Dr. Gias Uddin Ahmad, Professor and Head, Department of Physics, Bangladesh University of Engineering and Technology (BUET) and Dr. A.A. Ziauddin Ahmad, Chairman, Space Research and Remote Sensing Organization (SPARRSO), Agargaon, Dhaka, for their constant guidance and supervision throughout the progress of this work.

Almost the entire work has been done in the Reactor and Neutron Physics Division (RNPd), Institute of Nuclear Science and Technology (INST), of the Atomic Energy Research Establishment (AERE), Savar, Dhaka. The author wishes to convey his deep gratitude to the Director, INST & specially to Dr. M. Azizur Rahman, Head, RNPd, INST, for extending laboratory facilities for carrying out the work and for constant encouragement and many useful suggestions.

The author is indebted to Dr. Farid Uddin Ahmed, Principal Scientific Officer, INST, for his keen interest, encouragement and many valuable discussions and suggestions.

The author wishes to take this opportunity in extending his gratitude to all members of RNPd, INST, specially to Mr. Imtiaz Kamal, Assistant Engineer, for their continuous assistance in the design of the monochromator drum and for carrying out the

experiment. The author expresses his sincere gratitude to Prof. M.A. Asgar, Prof. T. Hossain and others of the Department of Physics, BUET, for their keen interest in the work and constant encouragement.

The author is grateful to Dr. M.A. Mannan, Chairman, Bangladesh Atomic Energy Commission, (BAEC); Dr. S.M.M.R. Chowdhury, Member, Physical Science, BAEC; Dr. M. Serajul Islam, Director General, AERE, BAEC, Savar, Dhaka, for their encouragement and interest.

The author wishes to express his gratitude to BUET and to BAEC for extending financial assistance and technical and laboratory facilities during the course of this work without which this thesis would not have been possible.

The secretarial assistance of Mr. Ali Hossain is thankfully acknowledged.

ABSTRACT

A monochromator drum of the proposed two-axis neutron spectrometer around the 3MW TRIGA Mark II research reactor at AERE, Savar has been designed. The shielding materials of the monochromator drum have been fabricated along with its associated equipment. The design principles of the monochromator drum were aimed at minimizing the cost by using locally available materials and gaining the maximum intensity of the neutron flux. For the evaluation of the shielding effectiveness of the shielding materials of the monochromator drum, different parameters such as neutron removal cross-section, gamma-ray attenuation co-efficient, relaxation length and build-up factor have been measured by using a ^{252}Cf source (nearly 1 μg). The integrated intensity at the sample position of a diffractometer and optimization of the parameters of the monochromator crystal are discussed. The integrated intensities at sample position have been calculated as a function of thickness and mosaic spread of a copper(Cu) monochromator (200) for different neutron wavelengths by using a computer code MONREF developed by H.A. Graf. The geometry of the neutron diffractometer has been taken from the proposed design of a double-axis neutron diffractometer at 3MW TRIGA Mark II research reactor at AERE, Savar, Dhaka. Optimum thickness and mosaic spread for the (200) plane of Cu monochromator at different neutron wavelengths have been determined through these calculations.

CONTENTS

	<u>Page</u>
CHAPTER 1 INTRODUCTION	1
CHAPTER 2 DESIGN AND FABRICATION OF A MONOCHROMATOR DRUM	
2.1 INTRODUCTION	4
2.2 DESIGN AND FABRICATION	5
2.3 MATERIALS	9
CHAPTER 3 SHIELDING EFFECTIVENESS OF A MONOCHROMATOR DRUM	
3.1 INTRODUCTION	18
3.2 THEORY	23
3.3 EXPERIMENT	31
3.4 RESULTS AND DISCUSSIONS	39
CHAPTER 4 OPTIMIZATION OF A MONOCHROMATOR CRYSTAL	
4.1 INTRODUCTION	63
4.2 DIFFRACTOMETER GEOMETRY	64
4.3 THEORY	65
4.4 RESULTS AND DISCUSSIONS	68
CHAPTER 5 CONCLUSIONS	79
REFERENCES	83
APPENDIX	86

CHAPTER 1
INTRODUCTION

INTRODUCTION



With the advent of nuclear reactors, neutrons have been made available in sufficient intensity to allow collimation into beams and segregation in energy within a fairly narrow band. Elsasser⁽¹⁾ first suggested that the motion of neutrons would be determined by wave mechanics, so that they would be diffracted by crystalline materials and shortly afterwards, an experimental determination of this was given both by Halban and Preiswerk⁽²⁾ and by Mitchell and Powers⁽³⁾. These experiments were done using a radium-beryllium neutron source, the neutrons from which were by no means of constant velocity, or 'monochromatic' and while sufficient to demonstrate that diffraction occurred, they were by no means sufficient to provide any quantitative data. The first apparatus of this sort usually termed a 'neutron spectrometer' although 'diffractometer' would be more accurate, was built at the Argonne National Laboratory in the U.S.A. in 1945 (Zinn⁽⁴⁾).

Neutron scattering is a versatile technique for the study of different aspects of materials. This is a complementary technique along with the other techniques used in applied materials science such as electron microscopy, x-ray, nuclear magnetic resonance, Raman spectroscopy, etc. A programme of neutron scattering work is being chalked out utilizing the neutron beam of the 3MW TRIGA Mark II research reactor at Atomic Energy Research Establishment (AERE), Savar, Dhaka under the Bangladesh Atomic Energy Commission (BAEC). A double-axis neutron diffraction spectrometer for elastic

scattering of neutrons has been designed and its fabrication is being carried out in phases at the 3 MW TRIGA Mark II research reactor at AERE, BAEC, Savar, Dhaka. A radial beam port of the research reactor has been chosen. The schematic diagram of a double-axis neutron diffraction spectrometer is shown in Figure 1. The design principles employed are aimed at mechanical and electrical simplicity, flexibility in operation and ease of fabrication. The proposed monochromator drum is the main component of the double-axis neutron diffraction spectrometer. The primary objective of the design of a monochromator drum was directed towards minimum cost and fabrication of the components with mostly locally available materials. Due to the limitations of the workshop facilities, manual control system has been adopted. The description of design and fabrication of a monochromator drum is given in Chapter 2.

The shielding effectiveness of five types of materials used in the monochromator drum have been measured using a mixed beam of neutrons and gamma rays from a ^{252}Cf source. The emission characteristic of ^{252}Cf source is similar to that inside a reactor core. The shielding effectiveness of these shielding materials is discussed in Chapter 3.

It is necessary to collimate the reactor neutron beam to have an excellent monochromatic beam. The purpose of the primary collimator is to produce the parallel neutron beam behind the monochromator crystal. The soller collimators are used to reduce the divergence

of the incident and reflected neutron beam behind and in front of the monochromator crystal. A copper (200) crystal has been used as the monochromator which will extract a monochromatic neutron beam by Bragg reflections from the Maxwellian distribution of neutrons emerging from the reactor. Some calculations on a copper monochromator have been carried out by H.A. Graf⁽⁵⁾ using his computer program MONREF for a particular diffractometer geometry. The program MONREF has been modified to calculate the quantitative angle at full-width at half maximum (FWHM), energy resolution at the sample position and intensity distribution over energy⁽⁶⁾. The quantitative resolution functions at the sample position have been calculated for different collimation angles of the soller collimator in front of and behind the Cu (200) monochromator for a geometry of the proposed diffractometer⁽⁷⁾. Chapter 4 describes the optimization of the monochromator crystal.

The purpose of the monochromator drum is to absorb all unwanted radiation to protect the personnel working around and to reduce the neutron background at the detector. The aim of the present work is to design a monochromator drum to be used with the double-axis neutron diffraction spectrometer at TRIGA Mark II research reactor at AERE, Savar, Dhaka, Bangladesh.

CHAPTER 2

DESIGN AND FABRICATION OF A MONOCHROMATOR DRUM

2.1 INTRODUCTION

The monochromator drum is the main component of the proposed double-axis neutron spectrometer to be built at a radial beam port of TRIGA Mark II research reactor of AERE, Savar, Dhaka, Bangladesh. The drum serves a variety of purposes for the experimenters in the field of neutron scattering. The shielding arrangement of the drum has to be such that all the unwanted portions of the reactor beam except the monochromated neutron beam taken out through the exit port have to be totally absorbed. This is necessary for the safety of the experimenters and also for the reduction of background at the neutron detector.

The shielding materials in the drum consists of lead (for gamma rays), stainless steel (for partial attenuation of fast and epithermal neutrons), borated paraffin (for slowing down of fast neutrons and subsequent capture) and ilmenite-magnetite concrete (for gamma rays and neutrons). Unlike other monochromator drums^(8,9), the vertical axis of the present monochromator has been placed nearest to the reactor wall in order to gain maximum neutron flux at the monochromator crystal and to save space vis-avis shielding materials. The monochromator copper crystal is placed in a steel frame hung by a rod from the top plug. The rod can be rotated about a vertical axis by a reduction gear. The precision of rotation is about 0.1° . A tilting mechanism around the horizontal plane has also been provided in the steel frame to keep the neutron beam in the horizontal plane.

The take-off exit port for the monochromatic neutron beam is kept fixed for a specific experiment. The exit port can be changed to other limited desired angle by taking off the shielding materials from the side of the port to which it is to be moved. This is why movable shielding blocks of appropriate shapes have been fabricated. Though this is a laborious work, it reduces the cost and complexity of fabrication of the components.

Wooden collimator having inner dimension suitable to specific experiment may be placed in the exit port. For this a number of wooden collimator having variable inner dimension have been built. The wooden collimators are covered with mild steel to bear the load of the shielding materials. Shielding dimensions were calculated by the following approximate method: Geometries were regarded cylindrical; source strengths could be calculated for fast neutrons (energies about 2 MeV) and gamma radiation (of an average hardness appropriate to gamma radiation from a reactor) from measured beam intensities and the beam geometry. The factor may be expressed in terms of the thickness of the material required for an attenuation of the order of 10^{-1} , and the thickness used for lead, borated paraffin, stainless steel and ilmenite-magnetite concrete were 18, 50, 1.5 and 20 cm respectively. The design and fabrication of the monochromator drum or house for the two-axis neutron spectrometer is described in Section 2.2.

2.2 DESIGN AND FABRICATION

Monochromator drum plays an important role in the proposed double-

axis neutron spectrometer. The front sectional view of a monochromator drum is shown in Figure 2. The monochromator drum comprises three parts collimator arrangement, sample table and shielding arrangement. The top sectional view of a monochromator drum is shown in Figure 3.

The primary or "inpile" collimator has inner square dimension of 5 cm X 5 cm and outer square dimension of 8cm X 8cm. The outside diameter and length of this collimator are 20.0 cm and 100 cm. respectively. Different sectional views of the primary collimator of the spectrometer are shown in Figure 4. A provision has been kept in the collimator to insert sollar slits for reducing angular divergence of neutron beams thereby increasing the resolution. At both ends of the collimator, 6 balls with springs underneath have been fitted so that the collimator can be pushed in and pulled out of the reactor beam port. A set of horizontal trays (not shown) has been provided at the end of the collimator facing the reactor core so that the boron of the borated paraffin will remain in the trays even if melting of paraffin wax occurs and this will help keep the homogeneity of the borated paraffin to some extent. The horizontal and vertical divergences of the primary collimator without sollar slits are determined by the ratio d/l of the width d and length l of the collimator.

Generally three collimators are used in a crystal spectrometer, the first one known as the primary collimator is located inside the beam port in the reactor shielding; the second one stands on the

monochromatic beam between the monochromator crystal and the sample table; the third one is on the rotating arm between the sample table and BF_3 detector. Our second and third collimators will be of the soller type⁽¹⁰⁾. The horizontal angular divergence of these collimators is determined by the ratio $\alpha = s/l$ of the width to the length l of its soller elements. Following Sailor et al.⁽¹¹⁾, it will be assumed that the transmission function of the monochromator, analyser and soller-slit system are Gaussian. According to Sailor et al., a soller collimator reduces the intensity of the incident beam by a factor

$$I(\Phi) = \exp \left[- (\Phi / \alpha')^2 \right] \quad (1)$$

where Φ is the angle made by the projection on a horizontal plane, of any individual ray with the central line of the collimator and α' is given by

$$\alpha' = \frac{\alpha}{2(\ln 2)^{1/2}} \quad (2)$$

The sign of Φ is chosen so that $+\Phi$ would tend to increase the Bragg angle of the ray. It has been shown by Caglioti et al.⁽¹²⁾, that by providing a coarse vertical collimation, any effect due to the vertical angular divergence of the collimator can be neglected.

The sample table rests on a semicircular rail concentric to the monochromator and can be rotated to any desired position/angle by a spur and worm gear. The reduction ratio of the spur and worm gear

is 30:1. The crystal rotating mechanism is shown in Figure 2. The sample table is connected with the rotating mechanism system by means of a long brass rod. The sample table can also be moved towards or away from the monochromator crystal so that the sample can be moved to the focal point of the crystal. The detector assembly is coupled to the sample table and can be rotated around the vertical axis of the sample table by a reduction gear. The precision of rotation is about 0.1° . A tilting mechanism around the horizontal plane has also been provided in the steel frame to keep the neutron beam in the horizontal plane. There is also provision to adjust the detector distance from the sample table. The beam stop also moves along a circular rail placed behind the sample table and the detector assembly concentric to the monochromator. The beam stop serves to slowing down of neutrons and subsequent capture and absorption of gamma rays.

The neutron and gamma ray shielding effectiveness of the different layers of the monochromator drum have been measured by using a 252-Cf source of strength about 1 μ g. The shielding effectiveness measurements suggest that 18 cm of lead, 50 cm of borated paraffin, 1.5 cm of stainless steel and 20 cm of ilmenite-magnetite concrete in the shape of circular rings are to be built around monochromator for the attenuation respectively of gamma rays, the slowing down of fast neutrons and their subsequent capture, the partial attenuation of fast and epithermal neutrons and the attenuation of gamma-rays and neutrons. So, design of the monochromator drum on the basis of these measurements will meet up our purpose because the thermal and

epithermal neutrons have more attenuation than fast neutrons in our shielding matrix. This indicates that we are on a safer side in designing the shielding considering fast neutron flux.

2.3 MATERIALS

The reduction of radiation intensities is accomplished through interaction of radiation with matter. The most significant radiations for which shielding is required are (i) the mixed radiation field consisting of the primary gamma-rays and neutrons present inside a research reactor and neutron generator and also those gamma-rays emitted by certain radioactive sources and (ii) the secondary gamma-rays produced by inelastic scattering of fast neutrons with shielding materials and the capture of thermal neutrons. The shield design involves more than choosing a suitable material (or materials) and determining the optimum thickness required to decrease the total radiation to an acceptable level. Elements of high atomic number and high density are the best for absorbing gamma rays and elements of low atomic number are the best for attenuation of neutrons. Heavy elements may be used also to slow down high energy neutrons by inelastic scattering. Hydrogenous materials i.e., materials containing hydrogen may be used to moderate intermediate neutrons. Neutron poisons, such as boron, may be used to absorb low energy neutrons without emitting high energy gamma-ray. In addition to possessing good attenuation properties, an ideal shielding material should have the following characteristics:

- o be inexpensive;

- o easy to handle and fabricate;
 - o physically strong and durable under operating conditions;
 - o stable in chemical composition and physical dimensions;
 - o fire-resistant;
 - o noncorrosive, nontoxic, and odorless;
 - o not affected by intense radiation fields or high temperatures;
- and
- o co-efficients of expansion that are compatible with other materials.

Since no material could have all these qualities, compromises in design and fabrication of mixed radiation shields are required. Materials used in the monochromator drum for the shielding purposes are (a) Lead (b) Ilmenite-Magnetite Concrete (c) Stainless Steel and (d) Borated Paraffin.

(a) Lead: Lead is the most widely used material for the construction of monochromator shields. Because of its high density and large atomic number, it is an efficient attenuator for gamma-rays upto an energy of 0.5 MeV where the photoelectric effect dominates. It is also an effective attenuator for relatively strong gamma-rays from external sources. Because of its high density, thickness of just a few centimeters of lead will provide a large reduction in the intensity of the strong gamma rays. Lead is widely used in the form of rectangular "bricks" in the construction of simple gamma ray shields. Potential problems due to streaming through cracks between the bricks can be overcome by building the

shield with multiple layers or by using specially shaped bricks with interlocking surfaces. Lead is also cast relatively easily into solid shapes, although some care must be taken in the casting process to avoid porosity or voids in the solidified shields.

(b) Ilmenite-Magnetite Concrete: Ordinary concrete is often used in the construction of large-volume shields, because of its low-cost. It is therefore most commonly used as the outer constituent of a shield lined with successive layers of steel, lead or other shielding materials. Although ordinary concrete consists mainly of water and low z elements, a special concrete known as 'Ilmenite-Magnetite' concrete contains a significant percentage of heavy components, and is therefore much more effective in gamma-ray shielding^[18].

A series of experiments^[13] performed with different types of concrete reveal that ilmenite-magnetite (I-M) and ordinary sand mixed together in the ratio 2:2:1 respectively produces the desirable results for reactor shielding. It is found that while density increases with the incorporation of ilmenite and magnetite, the structural properties like compressive strength deteriorates. To summarize, the density of ordinary concrete is 2.226 g/c.c. with 4120 psi (12" X 6" cylinder) compressive strength while the I-M concrete has the density 2.95 g/c.c. with 3990 psi (12" X 6" cylinder) compressive strength^[18]. The final form of the composition of the I-M concrete is given in Table 1. The development of this special concrete is made in connection with the

construction of the biological shielding of the 3 MW TRIGA Mark II research reactor, AERE, Savar, Dhaka. The vendor's (General Atomic Inc., San Diego, USA) requirement was 2.755 g/c.c. with 3000 psi (12" X 6" cylinder) compressive strength. Hence, the I-M concrete as described above seems to be the best compromise for use as reactor shielding material.

(c) Stainless Steel: Steel is a good shield for epithermal and MeV energy neutrons. Iron or stainless steel or mild steel is also a common gamma-ray shielding material. Because both the atomic number and density of stainless steel are considerably lower than those of lead, thickness of several tens of centimeters are normally required for even very low energy gamma-rays. It is often used in situations where the size or configuration of the shield would make its construction from lead alone too expensive. In such circumstances, an outer layer of stainless steel with an inner lead lining is often an effective compromise.

(d) Borated paraffin: It is well known that neutrons are most effectively moderated by hydrogenous materials. Addition of boron in hydrogenous materials gives extra advantage, providing good absorption of neutrons and reducing secondary gamma radiation, which result in desirable neutron shielding characteristics. The neutron shielding material named 'Borated paraffin' has some unique properties and is found to have good neutron shielding properties. There are a number of materials like polyethylene and paraffin wax which contain more hydrogen per unit volume than water and at the

same time have lower density. These two materials together produce a matrix with desirable nuclear and structural properties.

The present development of the borated paraffin is unique in the sense that it has been ensured to have a uniform distribution of boron content in the shielding medium. The preparation process of the developed shielding material borated paraffin is described as follows: At first some quantity of paraffin wax is taken in a container for heating. It melts at about 80°C . After completion of the melting of paraffin wax, some quantity of boric acid is poured into the container and stirred constantly. The melting point of boric acid is higher than that of paraffin wax. So, constant heating along with stirring is necessary to still greater extent. It must be ensured that boric acid and paraffin wax are mixed uniformly. Then some granules of polyethylene are poured into the mixture of paraffin wax and boric acid. The melting point of polyethylene is higher than that of boric acid. So, more constant heat should be applied for melting the polyethylene. Constant stirring and heating for about an hour, three substances mix together uniformly. Then, the mixture is cooled down for resolidification. Hence, in borated paraffin material, the boron content is not segregated by melting and resolidification process.

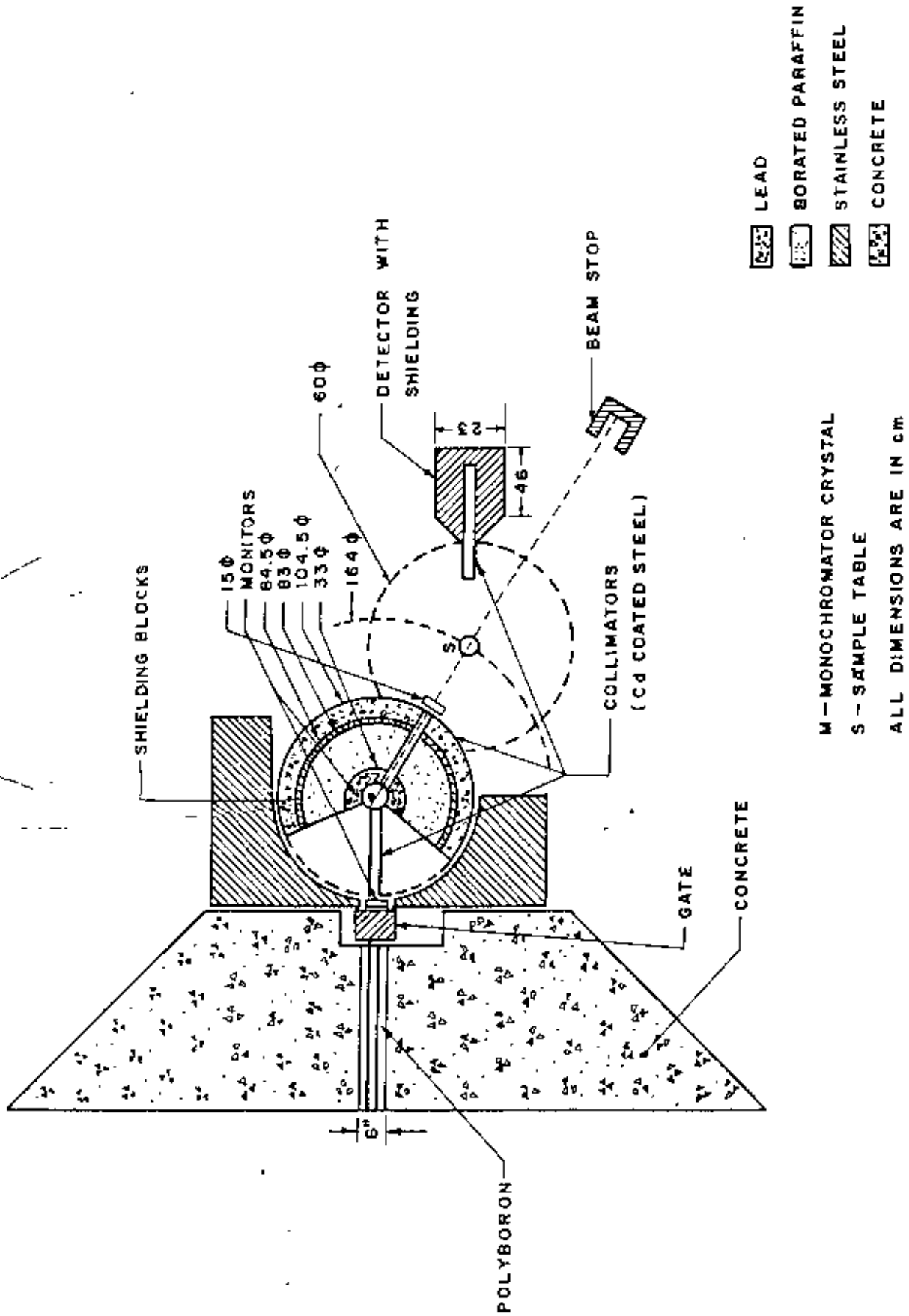
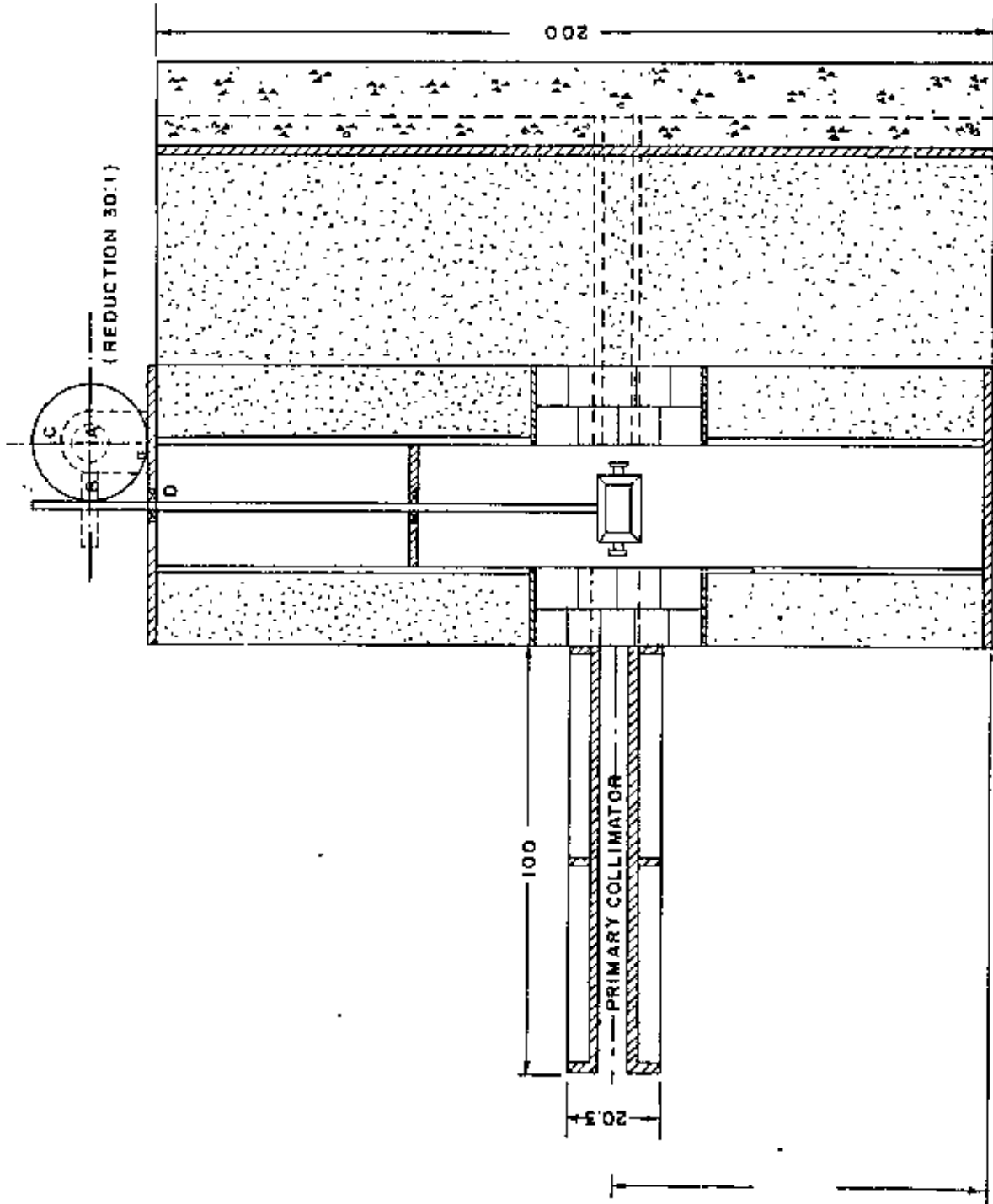


FIG. 1. SCHEMATIC DIAGRAM OF A 2 AXIS NEUTRON DIFFRACTOMETER.



FRONT SECTIONAL VIEW (A-A)
 (MONOCHROMATOR DRUM)

FIG. 2. THE FRONT SECTIONAL VIEW OF A MONOCHROMATOR DRUM.

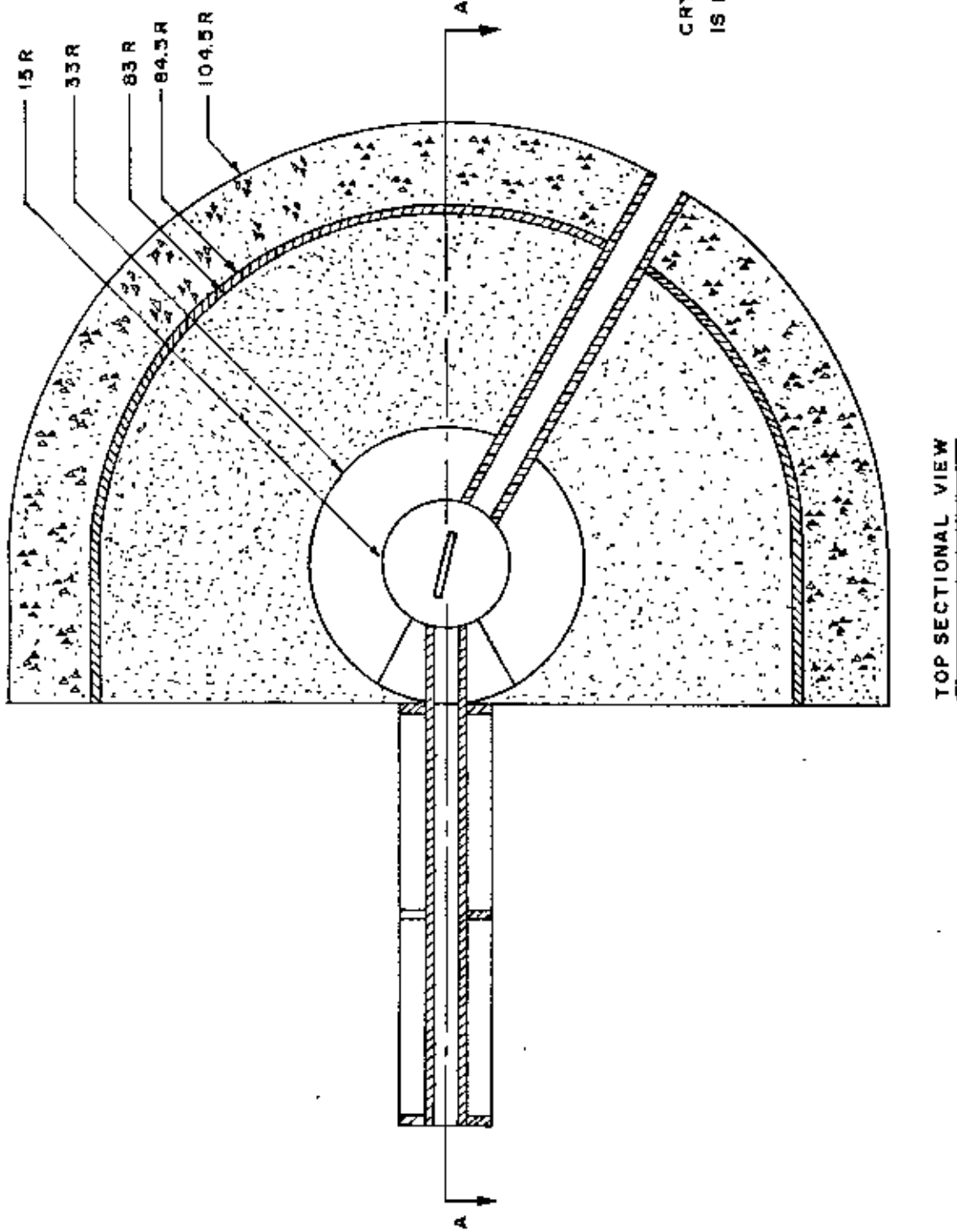
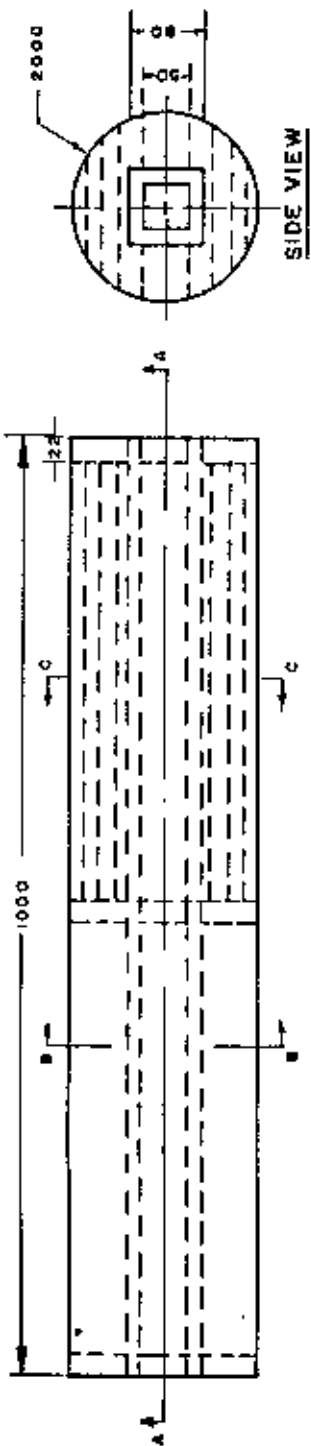


Fig. 3. THE TOP SECTIONAL VIEW OF A MONOCHROMATOR DRUM

ASSEMBLY DRAWING OF NEUTRON SCATTERING COLLIMATOR

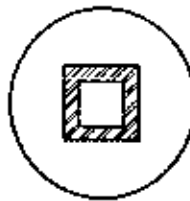


TOP VIEW

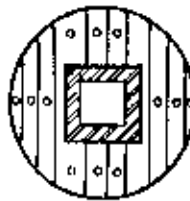
SIDE VIEW



SECTIONAL VIEW A-A



SECTIONAL VIEW B-B SECTIONAL VIEW C-C



ALL DIMENSION ARE IN mm
SCALE 1mm = 5 mm


 MILD STEEL

Fig. 4. DIFFERENT SECTIONAL VIEWS OF THE PRIMARY COLLIMATOR OF THE DIFFRACTOMETER

CHAPTER 3

SHIELDING EFFECTIVENESS OF A MONOCHROMATOR DRUM

3.1 INTRODUCTION

In principle, the radiations which might escape from a reactor include alpha and beta particles, gamma rays, neutrons of various energies, fission fragments, and even protons resulting from (n,p) reactions. The shield which protects personnel from these radiations is referred to as the biological shield⁽¹⁴⁾. As far as shield design is concerned, however, only gamma rays and neutrons need to be considered since there are by far the most penetrating. Any material which attenuates these radiations to a sufficient extent will automatically reduce all the others to negligible proportions. For the purpose of shield design, the neutrons and gamma rays are considered from the standpoint of their place of origin: the primary radiations are defined as the radiation which originate within the reactor core due to the nuclear fission, whereas the secondary radiations are produced outside the core as a result of the interaction of the primary radiations, chiefly the neutrons with nuclei in the reflector, coolant and shield materials. In this case, the radiation consists of a mixture of both gamma-rays and neutrons. As we have seen, elements of high atomic number are best for attenuation of gamma rays and elements of low atomic number are best for attenuation of neutrons. So that there is no one element which is good for both gamma rays and neutrons. For this reason, the shield for a mixed radiation field must consist of a suitable mixture of heavy and light materials.

Neutron shielding is mainly concerned with the behaviour of fast neutrons in matter rather than with the behaviour of average

neutrons, as in measurement of diffusion lengths, Fermi age, buckling etc. Broadly speaking, the absorption of fast neutrons is a two-step process: (i) the neutrons are slowed principally by elastic and inelastic collisions, with few captures occurring at high energies; and (ii) the moderated neutrons are effectively removed by capture because of the much higher cross-section at lower energies. The attenuation of neutrons may be summarised in the following manner: at first, a high energy neutron passes through the absorber material and is slowed down by elastic or inelastic scattering. When the neutron has been slowed down to thermal energy, probability of capture reaction increases and the neutron will be completely absorbed with the emission of either a charged particle or a gamma-ray having an energy upto several MeV. Since the neutron capture cross-sections for all materials is virtually zero at high energies, it is only when the neutron has reached sufficiently low energy that the capture of the neutron can take place. The probability of anyone of these events occurring in a material is expressed quantitatively by their respective cross-section. The cross-section may be either large or small depending on the neutron energy. Inelastic scattering is an important mechanism in the degradation of the energy of fast neutrons. The cross-section for this process increases with the neutron energy and with the atomic number of the material in which the scattering occurs. This is an important characteristic in the shielding against fast neutrons.

Elements of low mass number is often used as the shield for slowing

down neutrons of high energy, the cross-section for inelastic scattering is, however, small especially for elements of low mass number. It is then advantageous to utilize inelastic scattering by introducing an element (or elements) of moderate or high mass number. Hence, a combination of a moderately heavy or heavy element with hydrogen will effectively slow down even neutrons of very high energies. In this respect, boron either combined in water or in some other compound relatively rich in hydrogen, plays a very important role in the moderation of fast neutrons and in the subsequent capture. Hydrogenous materials combined with boron, provides good absorption of neutrons and also reduce secondary gamma radiation resulting from (n, γ) reaction.

Gamma-ray shielding is concerned with the behavior of gamma-ray in matter. Although a large number of possible interaction mechanism are known for gamma rays in matter, only three major types play an important role in radiation measurements: photoelectric absorption, Compton scattering and pair production. All of these processes lead to the partial or complete transfer of the gamma-ray energy to electron energy. In their passage through matter the gamma-ray photons are removed so that the intensity falls off in an exponential manner. Gamma-rays are most effectively attenuated by 'lead' because of its high density and large atomic number. Steel and concrete are also a common gamma-ray shielding material and are often used in situations where the size or configurations of the shield would make its construction from 'lead' alone too expensive. Because of its low cost, concrete is used in the construction of

large volume shields. Although ordinary concrete consists mainly of water and low Z elements, a special formulation known as ilmenite magnetite concrete contains a significant percentage of heavy components, like Fe, V, Ti, etc. and is, therefore, more effective in gamma-ray shielding.

Dubrovski et al.^[15] have studied the shielding properties of stone concretes by measuring the relaxation lengths and they concluded that the stone concretes (density 2.38g/cm^3) are more effective than the ordinary concretes (density 2.2g/cm^3). from the radiation shielding point of view. The attenuation of fast neutrons in ilmenite concrete has been studied by Adams and Lokan^[16,17]. The densities of concretes studied varied from 2.4 to 3.8g/cm^3 . No comparison has been made between ordinary concrete and ilmenite concrete. F.U. Ahmed et al.^[18] have studied the gamma ray shielding properties of ilmenite-magnetite (I.M) concrete and polyboron by measuring the instantaneous relaxation length and the spectral build-up factor using a ^{252}Cf source. Spectral build-up factor and instantaneous relaxation lengths have been fitted to the appropriate functions and the related co-efficient are also reported. Makarious et al.^[19] have studied the penetration of primary gamma ray, secondary gamma ray and slow neutrons through an ilmenite-limonite (2.9g/cm^3) shield and through both ordinary (2.3g/cm^3) and ilmenite concrete (4.6g/cm^3) shields. Ilmenite concrete is better than both ordinary and ilmenite-limonite concrete for attenuation of gamma and slow neutrons. Bhuiyan et al.^[20,21] have studied the neutron transport and shielding properties of locally

developed shielding material 'POLYBORON'. This developed material Polyboron has been patented in Bangladesh (Patent No. 1001787, Bangladesh Gazette No. 158/84, 1985). They measured the instantaneous relaxation length and effective removal cross-section as a function of penetration distance with and without cadmium sheet. F.U. Ahmed et. al⁽²²⁾ have measured the dose build-up factor (upto 20 mean free path) for gamma rays from a point isotropic ^{60}Co source penetrating multilayered concrete slabs using Cox's Bazar and Sylhet sands. They have also measured the instantaneous relaxation length for both types of concrete slabs. Results obtained show that the build up factors for Sylhet sand slabs increase more rapidly than those of magnetic slabs. Gujrathi and Dauria⁽²³⁾ have studied the attenuation of a fast (= 2.6 MeV) neutron beam by graphite, paraffin, polyethylene-boron, polyethylene-boron lead, polyethylene lithium and steel using an indirect method with a Ge (Li) gamma ray spectrometer. In addition, the macroscopic removal cross-section for these materials on the thermal neutron flux were also observed. Uwamino et al⁽²⁴⁾ have measured the attenuation of neutrons and photons transmitted through ordinary concrete. Source neutrons and photons were obtained from 252-Cf fission source.

Relative shielding properties of ammonia-meta-tungsten for neutrons and gamma rays from 252-Cf fission source have been studied by Senffle and Philbin⁽²⁵⁾.

The shielding effectiveness of materials such as lead, stainless

steel, borated paraffin and ilmenite-magnetite concrete contained in the monochromator drum against a spectrum of fast neutrons and gamma rays emanating from a ^{252}Cf source of strength about 1 μg will now be investigated.

3.2 THEORY

The neutrons emitted by the ^{252}Cf source is very similar to the neutrons generated in the core of an operating nuclear reactor. Their vast number, energy and potential for biological harm, constitute a major radiation hazard; their adequate attenuation is therefore a primary function of the reactor shield. There are two different modes by which neutrons may interact with matter. These are scattering and capture. When the neutrons are fast, there is a tendency for them to be slowed down by scattering processes. If the collisions are of the inelastic type, the process will be accompanied by emission of gamma rays. These produce a part of the secondary radiations which must be attenuated in the shield. After suffering a number of collision, the fast neutrons enter the energy region where they are readily captured. The resulting capture gamma rays make a major contribution to the secondary radiation. Furthermore, some of the capture products will be radioactive and emit beta particles, often accompanied by gamma rays. These and the bremsstrahlung produced by the interaction of the beta particles with nuclei add to the complexity of the secondary radiations in the shield, although the bremsstrahlung does not make any significant contribution to the radiation dose. Apart from the variety of the radiations, both in intensity and energy, the fact

that they are produced throughout the shield volume greatly increase the difficulty of making attenuation calculations⁽²⁵⁾. The magnitude of the problem arising from capture gamma rays in a shield can be decreased by the use of Boron-10, which has a large cross-section for the (n,α) reactions with slow neutrons. Some gamma-radiation accompanies the neutron absorption reaction, but its energy is only about 0.5 MeV and so it is easily attenuated. Proper location of boron in a shield can often result in a decrease in the overall shield thickness because of the low energy of the secondary gamma rays. Many of the neutrons escaping from the reactor are slowed down and captured by the boron, so that a smaller degree of attenuation is required in the remainder of the shield.

The important aspect of the shielding problem is the attenuation of the various gamma rays both primary and secondary. As far as their behaviour is concerned, the origin of these radiations is not significant; it is only the energy which determines the attenuation in a given medium. All substances will attenuate gamma rays to some extent, although the linear attenuation co-efficient (or macroscopic cross-section) generally increases with the density of the attenuating material. This co-efficient is very roughly proportional to the density and the thickness of different materials required to attenuate gamma radiations of specified energy, to the same extent, are inversely proportional to their respective densities. Consequently, where the thickness of the shield is an important consideration, a material of high density would be used to attenuate the gamma rays.

To evaluate the effectiveness of any new shielding material, the following nuclear parameters are to be considered:

- i) Attenuation co-efficient (μ)
- ii) Removal cross-section (Σ_r), generally for neutrons
- iii) Relaxation length (λ) and
- iv) Build-up factor (B)

Each of the term mentioned above is briefly described below:

- i) Attenuation co-efficient(μ)

The most important quantity characterizing the penetration and diffusion of gamma radiation in extended media is the attenuation co-efficient, μ . This quantity depends on the photon energy E and on the atomic number Z of the medium and may be defined as the probability per unit path length that a photon will interact with the medium. The rate at which gamma rays are attenuated is determined primarily by the atomic number and density of the shielding material, and to a lesser extent by its geometrical configuration. Let us consider a slab of material of thickness t located between a narrowly collimated beam of monoenergetic gamma ray photons and a narrowly collimated detector, as shown in Figure 5. The distinctive feature of a narrow beam experiment (i.e. one having, good geometry') is that only the photons which traverse the specimen absorber without experiencing an interaction of any kind, reach the detector, all other photons are prevented from reaching the detector. When monoenergetic gamma ray photons traverse a small thickness of slab at any point in a medium, the extent of interaction of the photons is proportional to the radiation intensity at that point and to the thickness traversed.

Consequently, in traversing the distance dt , the intensity of the gamma-ray photons which have not undergone interaction will be decreased by

$$dI/I = -\mu dt \quad (1a)$$

where μ is called the attenuation co-efficient of the absorber for the given radiation. Integrating equation (1a) and assuming that the beam intensity incident on the slab has the value $I(0)$, the intensity transmitted $I(t)$ through the slab of a homogeneous medium is given by

$$I(t) = I(0) e^{-\mu t} \quad (1b)$$

Equation 1(b) represents the attenuation of gamma rays in a material medium and is exponential in nature.

ii) Removal cross-section (Σ_R)

The removal cross-section of a material as used in the shielding calculations, is the cross-section which describes the probability that a neutron will reach a given detection point in a material without being absorbed or scattered out of the direct path. If t is the thickness of the material through which neutrons are passing, then (neglecting geometry effects) the ratio of the emergent (transmitted intensity), $I(t)$ to the incident intensity $I(0)$ is given by

$$I(t) = I(0) e^{-\Sigma_r t} \quad (1(c))$$

where Σ_r is the macroscopic removal cross-section for neutrons in the material, but it is not a cross-section in the sense of representing the probability of a particular neutron-nucleus interaction. The observed value of the removal cross-section is in fact, roughly equal to two-thirds of the total (scattering and capture) cross-section in the given material for neutrons having energies in the range of 6 to 8 MeV.

iii) Relaxation length (λ):

The relaxation length of any material is that thickness of material in which the incident radiation diminishes to a factor of $1/e$ (i.e. $[I(t)]/[I(0)] = 1/e = 0.37$) or to 37% of its incident intensity, where e is the base of natural logarithms. This factor is also called the mean free path (mfp), which represents the average distance traveled by a photon between successive interactions. If $I(t)$ is the radiation (neutron or gamma ray) flux or related quantity at a point t within a shield, then the relaxation length λ , for the given radiation and medium, is given by

$$\frac{1}{\lambda} = - \frac{1}{I(t)} \cdot \frac{dI(t)}{dt} \quad (1(d))$$

at the point t . As defined in this manner, the relaxation length may vary with the distance t within the shield. However, it is often found that, owing to a combination of circumstances, the radiation flux decreases in an approximately exponential manner

over a range of distances in the shield; over this range λ remains constant and the flux at t can be represented by

$$I(t) = I(0) e^{-t/\lambda} \quad (1e)$$

where $I(0)$ is the flux at the origin of the t co-ordinate. Comparison with the attenuation equation for gamma rays (1b) and equation for neutrons (1c) shows that λ is formally equivalent to $1/\mu$ or $1/\Sigma_r$, respectively. Since the relaxation length of a particular radiation in a given material is equivalent to the reciprocal of an attenuation co-efficient (for gamma rays) or a removal cross-section (for neutrons), it is dependent on the energy of the radiation. For a specified radiation of a given energy, the relaxation lengths (or their reciprocals) provide a rough means for comparing the shielding effectiveness of different materials. Relaxation lengths may also occasionally be used in very preliminary shielding calculations, but this procedure is not recommended unless there is a clear understanding that the results are highly approximate.

iv) Build-up factor (B):

In the exponential law (eqn 1b) for the attenuation of gamma-radiations in materials, it is assumed that the particular photon involved in a reaction such as photoelectric effect, compton scattering and pair production in the material is completely eliminated and is not seen by a detector output across the

shielding material. It is however, true only in the case of narrow beam geometry (Fig. 5a), the secondary radiations resulting from the interaction of primary photons in the material have every possibility to pass through the shield and thus the photon flux across the shield will be greater than that calculated from equation (1b). In the case of broad beams the equation (1b) will be modified to

$$I(t) = BI(0) e^{-\mu t} \quad (1f)$$

where B is the build-up factor and is defined as follows^[27]

$$B = \frac{\text{Quantity of interest at a point due to the total number of particles}}{\text{Quantity of interest at a point due only to non-interacted particles}}$$

The 'quantity of interest' might be the number of particles, their energy, or the dose imparted by them; thereby giving rise the number, energy, and dose build-up factors, respectively. The build-up factor, B, takes into account the increase in the radiation intensity due to scattering within the absorber, $I(0)$ is the initial intensity of the radiation source, $I(t)$ is the attenuated intensity after passing through the shielding materials of thickness t (cm) and μ is the attenuation co-efficient (cm^{-1}). If

all three types of interaction of gamma-ray photons with the matter are included, then

$$\mu = \mu_{pe} + \mu_c + \mu_{pp} \quad (1g)$$

where μ_{pe} , μ_c and μ_{pp} represent the attenuation co-efficients due to photoelectric, the Compton effect, and pair production respectively. Usually, build-up factors are given at different relaxation lengths or attenuation units, μt . Like the attenuation co-efficient, the value of the B varies with absorber material and radiation energy. It also varies with geometry of the source and depth of penetration in the absorbing material. The total attenuation co-efficient is calculated for a given energy by

$$\mu = \frac{0.693}{HVT} \quad (1h)$$

where HVT is the half value thickness. In practical gamma-ray shielding calculation, the build-up factor is being widely used to determine the total effect of the radiation at the point of interest. In principle, the build-up factor concept is also applicable to neutron attenuation, but in practice it is found to be much less successful when applied to neutrons, and consequently it is much less important concept in the context of neutron shielding calculation.

3.3 EXPERIMENT

The measurement of attenuation properties of neutrons and gamma-rays through different types of arrangement of shielding materials were carried out at the laboratory of the Institute of Nuclear Science and Technology (INST) of the Atomic Energy Research Establishment (AERE), Savar. In our experiment, the broad beam geometry was employed in order to include the maximum amount of scattered radiation in the transmitted beam, shown in Figure 5. A block diagram of the experimental arrangement for the attenuation measurement along with the schematic diagram is shown in Fig. 6. The experimental set up consists of a radiation source, a detector system and multilayer shielding materials. The distance between the source and the detector was 130 cm. for neutron and gamma-ray shielding arrangement. The detection system consists of two parts: a detector and a recording system. The incoming radiation interacts with the detector and gives rise to an output pulse. The recording system receives this output pulse and after proper amplification and subsequent discrimination, records the number of events. The method used for the detection of neutron and gamma radiation depends on the ionization produced in the detector in course of their passage through the gas and matter, respectively. Measurements of gamma-ray intensity were performed by using a NaI(Tl) scintillation detector. Measurements of neutron intensity were carried out by using a long counter, which was constructed following the design of Hanson-Mckibben⁽²⁸⁾ incorporating the modification of thickness of the paraffin moderator as suggested by other workers⁽²⁹⁾. The long counter used in this study was a BF₃ gas

proportional detector. Surrounded by cylindrical paraffin moderator to monitor neutron flux, its sensitivity is reasonable, uniform for neutron energies ranging from thermal to 10 MeV.⁽³⁰⁾ This device has proved to be highly successful as a neutron monitor in experiments using fast neutrons⁽³¹⁾. The operating voltage of the BF_3 gas proportional detector was 1750 volts (Fig. 7). The fine and coarse gain of amplifier of type 2012 were 64 and 0 respectively.

The incident neutron flux was first measured without any shielding slab between the source and the detector. Then, the first slab of the shielding material was placed nearest to the source and the transmitted intensity was measured by the detector. The next slabs were successively introduced in front of the slabs already existing. In this way, the shielding thickness was increased, while the rest of the geometry remain unchanged. The measurements were carried out up to the different slab-thickness for five different shielding materials. This helped to study the deep penetration behaviour of neutron for the material under investigation.

The experiment was carried out using ^{252}Cf fission source which emits both fission neutrons and fission gamma rays. The strength of the source used in this study was $1 \mu\text{gm}$; which corresponds to $2.3 \times 10^6 \text{ n/sec}/\mu\text{g}$ and $1.3 \times 10^7 \text{ photons/sec}/\mu\text{g}$. This source was chosen because of its fission yield being identical to the fission yield to ^{235}U which undergoes nuclear fission with thermal neutrons in a reactor core⁽³²⁾. The average neutron energy of the fission spectrum due to ^{252}Cf and ^{235}U have a mean values of 2-3 MeV and

2 MeV respectively. Some physical properties⁽³³⁾ of ^{252}Cf are summarized in Table 1. The specifications of BF_3 detector and $\text{NaI}(\text{Tl})$ detector are given in Table 2 and Table 3 respectively. The compositions and naming of the five different shielding materials are given in Table 4.

The experiment was repeated for gamma-ray shielding effectiveness. The high voltage supply to the $\text{NaI}(\text{Tl})$ detector was 700 volts. The fine and coarse amplifier gain were 0 and 8 respectively. These measurements were carried out upto the slab thickness of 68.5 cm, 35.5 cm, 44.4 cm, 80.0 cm and 50.0 cm for ST1, ST2, ST3, ST4 and ST5 respectively. The dimensions of the different types of slabs are shown in Table 5. Brief descriptions of some of the different shielding materials have already been given in Section 2.3.

Table 1: Physical properties of ^{252}Cf

Atomic number	98
Mass number	252
Half-life for alpha emission	2.72 years
Half-life for spontaneous emission	85.5 years
Half-life (effective)	2.65 years
Fraction of decay by alpha emission	97%
Fraction of decay by spontaneous fission	3%
Average number of neutrons per spontaneous fission	3.8
Decay heat (5% from fission, 49% from decay)	$39 \mu\text{W}/\mu\text{g}$
Specific activity	$530 \mu\text{Ci}/\mu\text{g}$
Neutron emission rate	$2.3 \times 10^6 \text{ s}^{-1} \mu\text{g}^{-1}$
Photon emission rate	$1.3 \times 10^7 \text{ s}^{-1} \mu\text{g}^{-1}$

Table 2: BF₃ detector specifications

Manufacturer	: Canberra Inc
Model	: 4528
Diameter	: 2.54 cm
Anode	: 0.005 cm diameter tungsten
End window	: 0.203 cm thick alumina (Al ₂ O ₃)
Filled gas	: BF ₃ (90% 10-B) at 120 cm Hg.
Active length	: 30 cm.
Outer shield	: 0.089 cm thick

Table 3: NaI (Tl) detector specifications

Dimension	: 7.6 cm X 7.6 cm
Window	: 0.05 mm aluminium (density: 147.9 mg/cm ³)
Reflector oxide	: 16 mm thick (density 88 mg/cm ³)
Magnetic/light shield	: Connecting lined steel
Bias	: 1000V
Resolution	: 7.5% at 662 KeV peak of 137-Cs

Table 4: Compositions and types of shielding materials

Names of the shielding materials	Compositions	Ratios	Referred to in the text as
1. Borated paraffin	A:B:C	3:1:1	ST1
2. Borated paraffin	A:B:C	3:2:1	ST2
3. Borated paraffin	A:C	3:1	ST3
4. Ilmenite-Magnetite	E:F;G	100:100:36	ST4
5. Lead	Lead	-	ST5

A: Paraffin Wax

E : Sand

B: Polyethylene

F: Aggregate

C: Boric Acid

G: Cement

Aggregate gradation:

Ordinary sand: Ilmenite: Magnetite:: 1:2:2

Table 5: Dimensions of the different types of slabs.

Type of slabs	Thickness (cm)	Width (cm)	Height (cm)
ST1	3.0	20	10
ST2	3.0	20	10
ST3	4.5	20	10
ST4	5.0	25.5	12.5
ST5	5.2	20	10

3.4 RESULTS AND DISCUSSIONS

The relative variation of neutron transmission factor $I/I(0)$, as a function of thickness for ST1, ST2, ST3, ST4 and ST5 are plotted in Figure 8. It is seen that ST2 shows more attenuation of neutron than those by other shielding materials, for small thickness. For an initial thickness of 7 cm, the attenuation of neutron observed for ST2 is 64% compared to 60.25%, 58.75%, 32.5% and 30.25% for ST1, ST3, ST4, and ST5 respectively. For the thickness of 28 cm, the attenuation of neutron increases to 91%, 88%, 87.5%, 87.25%, and 78% for ST1, ST2, ST3, ST4 and ST5 respectively. For thickness of 28 cm, it is evident that the neutron shielding effectiveness of ST2, ST3, and ST4 are almost same. The cause of higher attenuation of neutron in the ST2 than in the ST1 for small thickness is probably due to the presence of more polyethylene in ST2. At 35 cm, they became comparatively less effective and amount to about 93.25%, 91%, 89.5%, 89.5% and 79.5% for ST4, ST1, ST2, ST3 and ST5 respectively. The gamma ray attenuation curves for the ST1, ST2, ST3, ST4 and ST5 are shown in Figure 9. The curves show that the lead arrangement contribute more attenuation in gamma-ray transmission than those of other shielding materials. For the thickness of 7 cm, the attenuation of gamma-ray intensity observed is 83.5% for ST5 compared to 40.75%, 29.5%, 27.25%, and 27.27% for ST4, ST2, ST3 and ST1, respectively. At 35 cm, the attenuation increases to 91.75%, 88.75%, 79%, 80.5%, 77.5% for ST5, ST4, ST2, ST3 and ST1 respectively. The results show that lead shielding material i.e. ST5 has greater gamma-ray shielding effectiveness

than those of others. The higher gamma-ray attenuation in ST5 is probably due to the higher density of the material.

The experimental data for neutron and gamma-ray shielding are given in Table 6-10 and Table 11-15 respectively. The attenuation of neutron intensity is generally characterized by removal cross-section (Σ_r), relaxation length (λ) and the attenuation of gamma-ray intensity is generally characterized by attenuation coefficient (μ), relaxation length (λ) and build-up factor (B). The build-up factor of gamma-ray radiation arises due to the multiple scattering. The curves of build-up factor vs thickness for ST1, ST2, ST3, ST4 and ST5 are shown in Figure 10, 11, 12, 13, and 14 respectively. The ST4 has smaller relaxation length than those for ST1, ST2 and ST3. This indicates that I-M concrete i.e. ST4 has more scattering centres than those of ST1, ST2, and ST3, and obviously the build-up factors are higher for ST4 due to multiple scattering than those for ST1, ST2 and ST3.

In the same manner, ST5 has smaller relaxation length than that of ST4. This indicates that the ST5 has more scattering centres than that of ST4 and obviously the build-up factors are higher for ST5 due to multiple scattering than that of ST4.

The gamma attenuation co-efficient and neutron removal cross-section of different shielding materials are shown in Table 16. Since the relaxation length of a particular radiation in a given material is equivalent to the reciprocal of the gamma-ray

attenuation co-efficient and to the reciprocal of the neutron removal cross-section, the relaxation lengths provide a good means for comparing the shielding effectiveness of different shielding materials. From Table (16), it is evident that the neutron removal cross-section and relaxation length of ST2 are better than those of ST1, ST3, ST4 and ST5. The gamma-ray attenuation co-efficients and relaxation lengths for ST1, ST2, ST3, ST4 and ST5 were evaluated and their results are also shown in Table (16). As can be seen the gamma ray attenuation co-efficients and relaxation lengths for lead i.e. ST5 are better than those of ST1, ST2, ST3 and ST4. It is also seen that the gamma-ray attenuation co-efficients and relaxation lengths of ST4 are better than those of ST1, ST2 and ST3. The value of attenuation co-efficient for ST4 is twice as large as that of ST1, ST2 and ST3. The shielding performance of ST4 depends on the properties of component substances and by suitable choice of constituents, it is possible to increase the density of material and optimize the shielding characteristics for various types of radiation. The locally made ilmenite and magnetite concrete have great economical potential for use in a nuclear radiation field. It is therefore, concluded that ST5 (lead) and ST4 (I-M concrete) are more effective than those of ST1, ST2 and ST3 for gamma-ray shielding measurements and ST1, ST2 and ST3 are more effective than ST4 and ST5 for neutron shielding measurements.

Table 6: Experimental data of neutron radiation for ST1.

No. Of obs.	No. Of Bricks	Thick- ness cm	Cumula- tive thi- ckness cm	Average counts per minute	Counting ratio I/I_0	Removal cross- section cm^{-1}	Relaxation length cm
1	23	2.9	68.5	154	0.0436	$0.0457_{-4}^{+1.9 \times 10^{-4}}$	21.88 ± 0.29
2	22	3.1	65.6	177	0.0500	$0.0456_{-4}^{+1.9 \times 10^{-4}}$	21.93 ± 0.26
3	21	3.1	62.5	187	0.0530	$0.0469_{-4}^{+2.0 \times 10^{-4}}$	21.82 ± 0.25
4	20	2.9	59.4	221	0.0625	$0.0466_{-4}^{+2.1 \times 10^{-4}}$	21.45 ± 0.18
5	19	3.0	56.5	232	0.0656	$0.0482_{-4}^{+2.3 \times 10^{-4}}$	20.76 ± 0.15
6	18	3.2	53.5	233	0.0659	$0.0508_{-4}^{+2.6 \times 10^{-4}}$	19.69 ± 0.13
7	17	2.9	50.3	251	0.0710	$0.0525_{-4}^{+3.0 \times 10^{-4}}$	19.04 ± 0.11
8	16	3.0	47.4	262	0.0741	$0.0548_{-4}^{+3.3 \times 10^{-4}}$	18.24 ± 0.11
9	15	3.1	44.4	271	0.0766	$0.0578_{-4}^{+3.7 \times 10^{-4}}$	17.31 ± 0.11
10	14	3.0	41.3	298	0.0843	$0.0598_{-4}^{+4.0 \times 10^{-4}}$	16.72 ± 0.12
11	13	2.8	38.3	343	0.0998	$0.0608_{-4}^{+4.6 \times 10^{-4}}$	16.44 ± 0.12
12	12	3.2	35.5	342	0.0968	$0.0657_{-4}^{+5.2 \times 10^{-4}}$	15.22 ± 0.13
13	11	2.7	32.3	359	0.1016	$0.0707_{-4}^{+6.5 \times 10^{-4}}$	14.15 ± 0.14
14	10	2.8	29.6	379	0.1072	$0.0753_{-4}^{+6.9 \times 10^{-4}}$	13.28 ± 0.14
15	09	2.9	26.8	396	0.1120	$0.0815_{-4}^{+8.4 \times 10^{-4}}$	12.27 ± 0.15
16	08	2.9	23.9	432	0.1223	$0.0877_{-4}^{+9.6 \times 10^{-4}}$	11.40 ± 0.15
17	07	2.8	21.0	454	0.1284	$0.0975_{-3}^{+1.1 \times 10^{-3}}$	10.26 ± 0.12
18	06	3.1	18.2	537	0.1520	$0.1032_{-3}^{+1.4 \times 10^{-3}}$	9.69 ± 0.11
19	05	3.3	15.1	620	0.1754	$0.1149_{-3}^{+1.7 \times 10^{-3}}$	8.71 ± 0.10
20	04	3.0	11.8	753	0.2130	$0.1310_{-3}^{+2.0 \times 10^{-3}}$	7.63 ± 0.10
21	03	2.9	8.8	1065	0.3014	$0.1363_{-3}^{+2.0 \times 10^{-3}}$	7.34 ± 0.08
22	02	3.0	5.9	1601	0.4530	$0.1342_{-3}^{+1.9 \times 10^{-3}}$	7.45 ± 0.04
23	01	2.9	2.9	2546	0.7204	$0.1130_{-3}^{+2.4 \times 10^{-3}}$	8.84 ± 0.08
24	00	0.0	0.00	3534	1.0000	0.0000	

Table 7: Eperimental data of neutron radiation for ST2

No.Of obs.	No.Of Bricks	Thick- ness cm	Cumula- tive thi- ckness cm	Average counts per minute	Counting ratio I/I_0	Removal cross- section cm^{-1}	Relaxation length cm
1	B6	3.0	35.5	362	0.1051	0.0635 $\pm 5.8 \times 10^{-4}$	15.75 \pm 0.13
2	B5	3.0	32.5	391	0.1134	0.0670 $\pm 6.7 \times 10^{-4}$	14.93 \pm 0.14
3	B4	3.1	29.5	419	0.1216	0.0714 $\pm 9.4 \times 10^{-4}$	14.00 \pm 0.15
4	B3	2.9	26.4	452	0.1312	0.0769 $\pm 1.0 \times 10^{-3}$	13.00 \pm 0.16
5	B2	3.0	23.5	463	0.1344	0.0854 $\pm 1.5 \times 10^{-3}$	11.71 \pm 0.12
6	B1	3.1	20.5	498	0.1445	0.0944 $\pm 1.8 \times 10^{-3}$	10.60 \pm 0.10
7	A6	2.9	17.4	551	0.1599	0.1054 $\pm 2.0 \times 10^{-3}$	9.49 \pm 0.09
8	A5	2.9	14.5	628	0.182	0.1174 $\pm 2.2 \times 10^{-3}$	8.52 \pm 0.07
9	A4	2.9	11.6	770	0.2235	0.1292 $\pm 2.6 \times 10^{-3}$	7.74 \pm 0.08
10	A3	2.9	8.7	1037	0.3010	0.1380 $\pm 3.0 \times 10^{-3}$	7.24 \pm 0.08
11	A2	2.9	5.8	1488	0.4318	0.1448 $\pm 3.3 \times 10^{-3}$	6.91 \pm 0.06
12	A1	2.9	2.9	2330	0.6761	0.1350 $\pm 3.7 \times 10^{-3}$	7.41 \pm 0.07
13	0	0.0	0.0	3446	1.000	0.0000	

Table 8: Experimental data of neutron radiation for ST3.

No. Of obs.	No. Of Bricks	Thick- ness cm	Cumula- tive thi- ckness cm	Average counts per minute	Counting ratio I/I_0	Removal cross- section cm^{-1}	Relaxation length cm
1	10	4.5	44.4	288	0.0838	0.0558 $\pm 5.3 \times 10^{-4}$	17.92 ± 0.15
2	09	4.3	39.9	310	0.0903	0.0603 $\pm 5.4 \times 10^{-4}$	16.59 ± 0.14
3	08	4.8	35.6	351	0.1022	0.0641 $\pm 5.7 \times 10^{-4}$	15.61 ± 0.13
4	07	4.4	30.8	403	0.1174	0.0696 $\pm 6.0 \times 10^{-4}$	14.38 ± 0.14
5	06	4.5	26.4	431	0.1255	0.0786 $\pm 6.1 \times 10^{-4}$	12.72 ± 0.12
6	05	4.5	21.9	488	0.1421	0.0891 $\pm 7.6 \times 10^{-4}$	11.23 ± 0.09
7	04	4.2	17.4	579	0.1686	0.1023 $\pm 1.2 \times 10^{-3}$	9.77 ± 0.10
8	03	4.7	13.2	753	0.2192	0.1150 $\pm 1.6 \times 10^{-3}$	8.70 ± 0.10
9	02	4.1	8.5	1186	0.3454	0.1251 $\pm 1.6 \times 10^{-3}$	8.00 ± 0.06
10	01	4.4	4.4	2142	0.6238	0.1073 $\pm 1.8 \times 10^{-3}$	9.32 ± 0.09
11	00	0	0	3434	1.0000	0.0000	

Table 9: Eperimental data of neutron radiation for ST4.

No.Of obs.	No.Of Bricks	Thick- ness cm	Cumula- tive thi- ckness cm	Average counts per minute	Counting ratio I/I_0	Removal cross- section cm^{-1}	Relaxation length cm
1	20	5	100	53	0.0178	0.0403_{-4} $\pm 1.2 \times 10^{-4}$	24.81 ± 0.06
2	19	5	95	58	0.0194	0.0415_{-4} $\pm 1.2 \times 10^{-4}$	24.11 ± 0.06
3	18	5	90	65	0.0218	0.0425_{-4} $\pm 1.3 \times 10^{-4}$	23.52 ± 0.07
4	17	5	85	57	0.0191	0.0466_{-4} $\pm 1.6 \times 10^{-4}$	21.47 ± 0.08
5	16	5	80	61	0.0204	0.0486_{-4} $\pm 1.8 \times 10^{-4}$	20.56 ± 0.08
6	15	5	75	67	0.0224	0.0506_{-4} $\pm 1.9 \times 10^{-4}$	19.76 ± 0.09
7	14	5	70	64	0.0214	0.0549_{-4} $\pm 2.0 \times 10^{-4}$	18.22 ± 0.09
8	13	5	65	78	0.0261	0.0561_{-4} $\pm 2.2 \times 10^{-4}$	17.83 ± 0.10
9	12	5	60	75	0.0251	0.0614_{-4} $\pm 2.3 \times 10^{-4}$	16.29 ± 0.10
10	11	5	55	79	0.0265	0.0660_{-4} $\pm 2.4 \times 10^{-4}$	15.14 ± 0.10
11	10	5	50	88	0.0295	0.0705_{-4} $\pm 2.6 \times 10^{-4}$	14.19 ± 0.11
12	09	5	45	111	0.0372	0.0732_{-4} $\pm 2.7 \times 10^{-4}$	13.67 ± 0.11
13	08	5	40	142	0.0476	0.0761_{-4} $\pm 2.8 \times 10^{-4}$	13.13 ± 0.11
14	07	5	35	207	0.0693	0.0762_{-4} $\pm 2.8 \times 10^{-4}$	13.15 ± 0.11
15	06	5	30	317	0.1062	0.0748_{-4} $\pm 2.7 \times 10^{-4}$	13.38 ± 0.10
16	05	5	25	470	0.1575	0.0739_{-4} $\pm 2.5 \times 10^{-4}$	13.52 ± 0.09
17	04	5	20	725	0.2429	0.0708_{-4} $\pm 2.0 \times 10^{-4}$	14.13 ± 0.09
18	03	5	15	1098	0.3678	0.0667_{-4} $\pm 1.6 \times 10^{-4}$	15.00 ± 0.08
19	02	5	10	1701	0.5698	0.0562_{-4} $\pm 1.4 \times 10^{-4}$	17.78 ± 0.07
20	01	5	05	2461	0.8244	0.0386_{-4} $\pm 1.0 \times 10^{-4}$	25.90 ± 0.06
21	00	0	00	2985	1.0000	0.0000	

Table 10: Experimental data of neutron radiation for ST5.

No. Of obs.	No. Of Bricks	Thick- ness cm	Cumula- tive thi- ckness cm	Average counts per minute	Counting ratio I/I_0	Removal cross- section cm^{-1}	Relaxation length cm
1	23	2.4	54.3	422	0.1430	0.0358 $\pm 1.8 \times 10^{-4}$	27.92 ± 0.06
2	22	2.4	51.9	451	0.1528	0.0368 $\pm 2.0 \times 10^{-4}$	27.63 ± 0.07
3	21	2.3	49.5	455	0.1542	0.0378 $\pm 2.1 \times 10^{-4}$	26.48 ± 0.08
4	20	2.2	47.2	474	0.1607	0.0387 $\pm 2.0 \times 10^{-4}$	25.82 ± 0.08
5	19	2.1	45.0	493	0.1671	0.0398 $\pm 2.1 \times 10^{-4}$	25.15 ± 0.09
6	18	2.5	42.9	497	0.1685	0.0415 $\pm 2.2 \times 10^{-4}$	24.09 ± 0.09
7	17	2.5	40.4	520	0.1763	0.0429 $\pm 2.4 \times 10^{-4}$	23.28 ± 0.10
8	16	2.5	37.9	554	0.1878	0.0441 $\pm 2.3 \times 10^{-4}$	22.66 ± 0.10
9	15	2.4	35.4	562	0.1905	0.0468 $\pm 2.6 \times 10^{-4}$	21.35 ± 0.10
10	14	2.4	33.0	597	0.2024	0.0484 $\pm 2.4 \times 10^{-4}$	20.66 ± 0.11
11	13	2.2	30.6	611	0.2071	0.0515 $\pm 2.5 \times 10^{-4}$	19.44 ± 0.11
12	12	2.2	28.4	658	0.2230	0.0528 $\pm 2.3 \times 10^{-4}$	18.93 ± 0.12
13	11	2.5	26.2	670	0.2271	0.0566 $\pm 2.8 \times 10^{-4}$	17.68 ± 0.14
14	10	2.6	23.7	765	0.2593	0.0569 $\pm 2.9 \times 10^{-4}$	17.56 ± 0.14
15	09	2.4	21.1	818	0.2773	0.0608 $\pm 3.0 \times 10^{-4}$	16.45 ± 0.15
16	08	2.4	18.7	946	0.3207	0.0608 $\pm 2.9 \times 10^{-4}$	16.44 ± 0.15
17	07	2.4	16.3	1079	0.3658	0.0617 $\pm 2.7 \times 10^{-4}$	16.21 ± 0.14
18	06	2.7	13.0	1280	0.4339	0.0642 $\pm 2.6 \times 10^{-4}$	15.57 ± 0.13
19	05	2.4	11.2	1465	0.4966	0.0625 $\pm 2.5 \times 10^{-4}$	16.00 ± 0.13
20	04	2.4	8.8	1738	0.5891	0.0601 $\pm 2.0 \times 10^{-4}$	16.63 ± 0.10
21	03	2.0	6.4	2127	0.7210	0.0511 $\pm 1.8 \times 10^{-4}$	19.57 ± 0.09
22	02	2.2	4.4	2477	0.8396	0.0397 $\pm 1.5 \times 10^{-4}$	25.18 ± 0.08
23	01	2.2	2.2	2771	0.9393	0.0285 $\pm 1.4 \times 10^{-4}$	35.15 ± 0.07
24	00	0.0	0.0	2950	1.0000	0.0000	

Table 11: Eperimental data of gamma-radiation for ST1.

No. Of obs.	No. Of Bricks	Thick- ness cm	Cumula- tive thi- ckness cm	Average counts per minute	Counting ratio I/I_0	Removal cross- section cm^{-1}	Relaxation length cm	Build up factor 'B'
1	23	2.9	68.5	7414	0.0747	0.0378_{-4} $\pm 1.2 \times 10^{-4}$	26.43 ± 0.02	2.19
2	22	3.1	65.6	8203	0.0827	0.0380_{-4} $\pm 1.2 \times 10^{-4}$	26.34 ± 0.02	2.10
3	21	3.1	62.5	8673	0.0874	0.0390_{-6} $\pm 1.3 \times 10^{-6}$	25.65 ± 0.03	1.91
4	20	2.9	59.5	9687	0.0976	0.0392_{-6} $\pm 1.4 \times 10^{-6}$	25.54 ± 0.03	1.84
5	19	3.0	56.5	10229	0.1031	0.0402_{-6} $\pm 1.1 \times 10^{-6}$	24.87 ± 0.02	1.67
6	18	3.2	53.5	11174	0.1120	0.0408_{-6} $\pm 1.3 \times 10^{-6}$	24.50 ± 0.04	1.58
7	17	2.9	50.3	11893	0.1198	0.0418_{-4} $\pm 1.3 \times 10^{-4}$	23.95 ± 0.04	1.43
8	16	3.0	47.4	12671	0.1277	0.0434_{-4} $\pm 1.5 \times 10^{-4}$	23.03 ± 0.05	1.32
9	15	3.1	44.4	14160	0.1427	0.0439_{-4} $\pm 1.6 \times 10^{-4}$	22.80 ± 0.05	1.28
10	14	3.0	41.3	15348	0.1546	0.0452_{-4} $\pm 1.6 \times 10^{-4}$	22.13 ± 0.04	1.19
11	13	2.8	38.3	17201	0.1734	0.0458_{-4} $\pm 1.5 \times 10^{-4}$	21.86 ± 0.04	1.15
12	12	3.2	35.5	19397	0.1955	0.0460_{-4} $\pm 1.5 \times 10^{-4}$	21.75 ± 0.04	1.13
13	11	2.7	32.3	21442	0.2161	0.0474_{-4} $\pm 1.6 \times 10^{-4}$	21.08 ± 0.06	1.06
14	10	2.8	29.6	23604	0.2379	0.0485_{-4} $\pm 1.6 \times 10^{-4}$	20.61 ± 0.06	1.04
15	09	2.9	26.8	27292	0.2751	0.0482_{-4} $\pm 1.8 \times 10^{-4}$	20.76 ± 0.07	1.04
16	08	2.9	23.9	31164	0.3141	0.0485_{-4} $\pm 1.8 \times 10^{-4}$	20.64 ± 0.07	1.03
17	07	2.8	21.0	36117	0.3640	0.0481_{-4} $\pm 1.9 \times 10^{-4}$	20.78 ± 0.07	1.03
18	06	3.1	18.2	40377	0.4069	0.0493_{-4} $\pm 2.0 \times 10^{-4}$	20.30 ± 0.08	1.02
19	05	3.3	15.1	<u>47321</u>	0.4769	0.0490_{-4} $\pm 2.0 \times 10^{-4}$	20.39 ± 0.09	1.02
20	04	3.0	11.8	56649	0.5710	0.0475_{-4} $\pm 1.8 \times 10^{-4}$	21.05 ± 0.07	1.02
21	03	2.9	8.8	65910	0.6642	0.0465_{-4} $\pm 1.6 \times 10^{-4}$	21.51 ± 0.07	1.01
22	02	3.0	5.9	76275	0.7687	0.0446_{-4} $\pm 1.3 \times 10^{-4}$	22.43 ± 0.06	1.01
23	01	2.9	2.9	87165	0.8784	0.0447_{-4} $\pm 1.0 \times 10^{-4}$	22.38 ± 0.05	1.01
24	00	0.0	0.0	99227	1.0000	0.0000		1.00

Table 12: The experimental data of gamma-radiation for ST2.

No. Of obs.	No. Of Bricks	Thick-ness cm	Cumula- tive thi- ckness cm	Average counts per minute	Counting ratio I/I_0	Removal cross- section cm^{-1}	Relaxation length cm	Build up factor 'B'
1	B6	3.0	35.5	19881	0.1975	$0.0457 \pm 1.7 \times 10^{-4}$	21.88 ± 0.09	1.22
2	B5	3.0	32.5	23004	0.2285	$0.0454 \pm 1.5 \times 10^{-4}$	22.02 ± 0.08	1.21
3	B4	3.1	29.5	25219	0.2505	$0.0469 \pm 2.0 \times 10^{-4}$	21.31 ± 0.08	1.14
4	B3	2.9	26.4	28625	0.2843	$0.0476 \pm 2.1 \times 10^{-4}$	20.99 ± 0.07	1.10
5	B2	3.0	23.5	31605	0.3140	$0.0493 \pm 2.0 \times 10^{-4}$	20.28 ± 0.09	1.05
6	B1	3.1	20.5	36285	0.3604	$0.0498 \pm 2.2 \times 10^{-4}$	20.09 ± 0.10	1.03
7	A6	2.9	17.4	41746	0.4106	$0.0506 \pm 2.2 \times 10^{-4}$	19.77 ± 0.10	1.01
8	A5	2.9	14.5	48012	0.4769	$0.0511 \pm 2.3 \times 10^{-4}$	19.58 ± 0.11	1.00
9	A4	2.9	11.6	55580	0.5530	$0.0512 \pm 2.6 \times 10^{-4}$	19.52 ± 0.11	1.00
10	A3	2.9	8.7	64637	0.6420	$0.0509 \pm 2.7 \times 10^{-4}$	19.63 ± 0.10	1.00
11	A2	2.9	5.8	75757	0.7524	$0.0490 \pm 2.5 \times 10^{-4}$	20.39 ± 0.10	1.00
12	A1	2.9	2.9	88336	0.8774	$0.0451 \pm 2.4 \times 10^{-4}$	22.17 ± 0.10	1.00
13	0	0.0	0.0	100682	1.0000	0.0000		1.00

Table 13: Experimental data of gamma-radiation for ST3.

No. Of obs.	No. of Bricks	Thick- ness cm	Cumula- tive thi- ckness cm	Average counts per minute	Counting ratio I/I_0	Removal cross- section cm^{-1}	Relaxation length cm	Build up factor 'B'
1	10	4.5	44.4	16967	0.1684	$0.0401 \pm 2.2 \times 10^{-4}$	24.93 ± 0.17	1.27
2	09	4.3	39.9	19469	0.1933	$0.0412 \pm 2.4 \times 10^{-4}$	24.28 ± 0.17	1.19
3	08	4.8	35.6	22134	0.2197	$0.0426 \pm 2.5 \times 10^{-4}$	23.49 ± 0.16	1.11
4	07	4.4	30.8	26355	0.2616	$0.0435 \pm 2.5 \times 10^{-4}$	22.97 ± 0.13	1.06
5	06	4.5	26.4	31964	0.3173	$0.0435 \pm 2.2 \times 10^{-4}$	23.00 ± 0.14	1.04
6	05	4.5	21.9	37662	0.3739	$0.0449 \pm 2.2 \times 10^{-4}$	22.26 ± 0.16	1.02
7	04	4.2	17.4	45675	0.4534	$0.0455 \pm 2.3 \times 10^{-4}$	22.00 ± 0.12	1.01
8	03	4.7	13.2	55747	0.5534	$0.0448 \pm 2.6 \times 10^{-4}$	22.31 ± 0.18	1.01
9	02	4.1	8.5	68943	0.6844	$0.0446 \pm 2.5 \times 10^{-4}$	22.42 ± 0.17	1.01
10	01	4.4	4.4	83085	0.8248	$0.0438 \pm 1.6 \times 10^{-4}$	22.85 ± 0.15	1.01
11	00	0	0	100731	1.0000	0.0000		1.00

Table 14: Eperimental data of gamma-radiation for ST4.

No.Of obs.	No.of Bricks	Thick- ness cm	Cumula- tive thi- ckness cm	Average counts per minute	Counting ratio I/I_0	Removal cross- section cm^{-1}	Relaxation length cm	Build up factor 'B'
1	16	5	80	7653	0.0952	0.0294 $\pm 1.3 \times 10^{-4}$	34.01 ± 0.17	50.99
2	15	5	75	6731	0.0836	0.0331 $\pm 1.4 \times 10^{-4}$	30.23 ± 0.17	30.27
3	14	5	70	6511	0.0809	0.0359 $\pm 1.5 \times 10^{-4}$	27.85 ± 0.18	19.77
4	13	5	65	6515	0.0810	0.0387 $\pm 1.6 \times 10^{-4}$	25.86 ± 0.19	13.36
5	12	5	60	6361	0.0791	0.0423 $\pm 1.9 \times 10^{-4}$	23.65 ± 0.19	8.81
6	11	5	55	6511	0.0810	0.0457 $\pm 2.0 \times 10^{-4}$	21.88 ± 0.19	6.09
7	10	5	50	6509	0.0810	0.0503 $\pm 1.8 \times 10^{-4}$	19.89 ± 0.21	4.11
8	09	5	45	7321	0.0910	0.0533 $\pm 1.7 \times 10^{-4}$	18.78 ± 0.20	3.12
9	08	5	40	7925	0.0985	0.0579 $\pm 1.6 \times 10^{-4}$	17.26 ± 0.18	2.28
10	07	5	35	9095	0.1131	0.0623 $\pm 1.8 \times 10^{-4}$	16.06 ± 0.17	1.77
11	06	5	30	10895	0.1355	0.0666 $\pm 2.0 \times 10^{-4}$	15.01 ± 0.16	1.43
12	05	5	25	13799	0.1716	0.0705 $\pm 2.2 \times 10^{-4}$	14.18 ± 0.12	1.22
13	04	5	20	18096	0.2250	0.0746 $\pm 2.2 \times 10^{-4}$	13.41 ± 0.11	1.08
14	03	5	15	24965	0.3104	0.0780 $\pm 2.3 \times 10^{-4}$	12.82 ± 0.12	1.04
15	02	5	10	36590	0.4549	0.0786 $\pm 2.4 \times 10^{-4}$	12.73 ± 0.13	1.02
16	01	5	05	55497	0.6900	0.0742 $\pm 2.4 \times 10^{-4}$	13.48 ± 0.13	1.02
17	00	00	00	80425	1.0000	0.0000		1.00

Table 15: Experimental data of gamma-radiation for ST5.

No. Of obs.	No. Of Bricks	Thick-ness cm	Cumula- tive thi- ckness cm	Average counts per minute	Counting ratio I/I_0	Removal cross- section cm^{-1}	Relaxation length cm	Build up factor 'B'
1	20	2.5	50.0	5400	0.0716	0.0527	18.97 ± 0.21	9.8×10^5
2	19	2.5	47.5	5422	0.0720	$0.0554 \pm 2.4 \times 10^{-4}$	18.05 ± 0.20	3.0×10^5
3	18	2.5	45.0	5477	0.0727	$0.0583 \pm 2.4 \times 10^{-4}$	17.16 ± 0.21	9.6×10^7
4	17	2.5	42.5	5615	0.0745	$0.0611 \pm 2.5 \times 10^{-4}$	16.37 ± 0.21	3.0×10^7
5	16	2.5	40.0	5808	0.0771	$0.0640 \pm 2.6 \times 10^{-4}$	15.62 ± 0.22	9.9×10^6
6	15	2.5	37.5	6056	0.0804	$0.0672 \pm 2.3 \times 10^{-4}$	14.87 ± 0.15	3.2×10^6
7	14	2.5	35.0	6291	0.0835	$0.0709 \pm 2.5 \times 10^{-4}$	14.09 ± 0.15	1.0×10^6
8	13	2.5	32.5	6525	0.0866	$0.0753 \pm 3.0 \times 10^{-4}$	13.28 ± 0.15	3.4×10^5
9	12	2.5	30.0	6663	0.0884	$0.0809 \pm 2.9 \times 10^{-4}$	12.37 ± 0.14	1.0×10^5
10	11	2.5	27.5	7082	0.0940	$0.0859 \pm 2.7 \times 10^{-4}$	11.63 ± 0.14	3.5×10^4
11	10	2.5	25.0	7248	0.0962	$0.0937 \pm 2.8 \times 10^{-4}$	10.68 ± 0.11	1.1×10^4
12	09	2.5	22.5	7607	0.1009	$0.1019 \pm 2.9 \times 10^{-4}$	9.81 ± 0.13	3675
13	08	2.5	20.0	8003	0.1062	$0.1121 \pm 3.2 \times 10^{-4}$	8.92 ± 0.12	1204
14	07	2.5	17.5	8455	0.1122	$0.1250 \pm 3.4 \times 10^{-4}$	8.00 ± 0.12	396
15	06	2.5	15.0	8960	0.1189	$0.1419 \pm 3.0 \times 10^{-4}$	7.04 ± 0.13	131
16	05	2.5	12.5	9578	0.1271	$0.1650 \pm 4.1 \times 10^{-4}$	6.06 ± 0.14	43.50
17	04	2.5	10.0	10357	0.1374	$0.1985 \pm 5.0 \times 10^{-4}$	5.04 ± 0.12	14.60
18	03	2.5	7.5	11930	0.1583	$0.2458 \pm 6.5 \times 10^{-4}$	4.07 ± 0.10	5.25
19	02	2.5	5.0	14404	0.1911	$0.3310 \pm 7.0 \times 10^{-4}$	3.02 ± 0.10	1.97
20	01	2.5	2.5	23461	0.3113	$0.4668 \pm 7.8 \times 10^{-4}$	2.14 ± 0.10	1.00
21	00	0.0	0.0	75364	1.0000	0.0000		1.00

Table 16: Gamma-ray Attenuation co-efficients and neutron removal cross-sections of different materials.

Types of the shielding materials	Gamma-ray attenuation co-efficient cm^{-1}	Neutron Removal cross-section cm^{-1}	Relaxation length	
			Gamma-ray cm	Neutron cm
ST1	0.046 ± 0.002	0.126 ± 0.002	21.35 ± 0.4	7.90 ± 0.01
ST2	0.049 ± 0.003	0.139 ± 0.010	20.42 ± 0.5	7.20 ± 0.01
ST3	0.044 ± 0.003	0.116 ± 0.008	22.60 ± 0.3	8.64 ± 0.02
ST4	0.093 ± 0.005	0.051 ± 0.003	10.73 ± 0.8	19.54 ± 0.29
ST5	0.478 ± 0.009	0.048 ± 0.007	2.10 ± 0.02	20.67 ± 0.36
Polyboron ^(18,20)	0.047 ± 0.004	0.161 ± 0.010	21.3 ± 0.4	6.25 ± 0.1

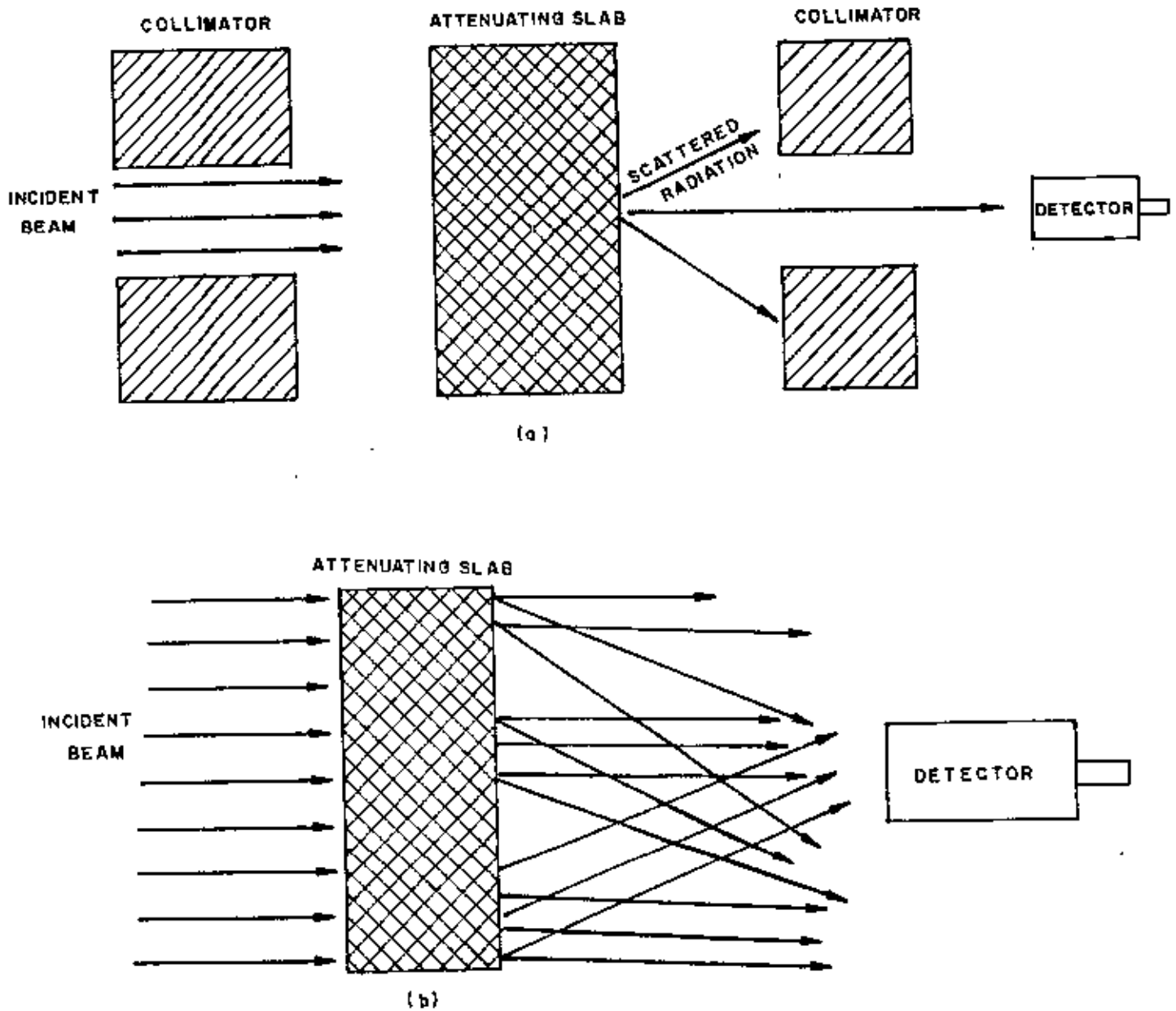


Fig. 5. EXPERIMENTAL ARRANGEMENTS FOR MEASUREMENTS OF ATTENUATION COEFFICIENT
 (a) NARROW BEAM OR GOOD GEOMETRY (b) BROAD BEAM OR POOR GEOMETRY.

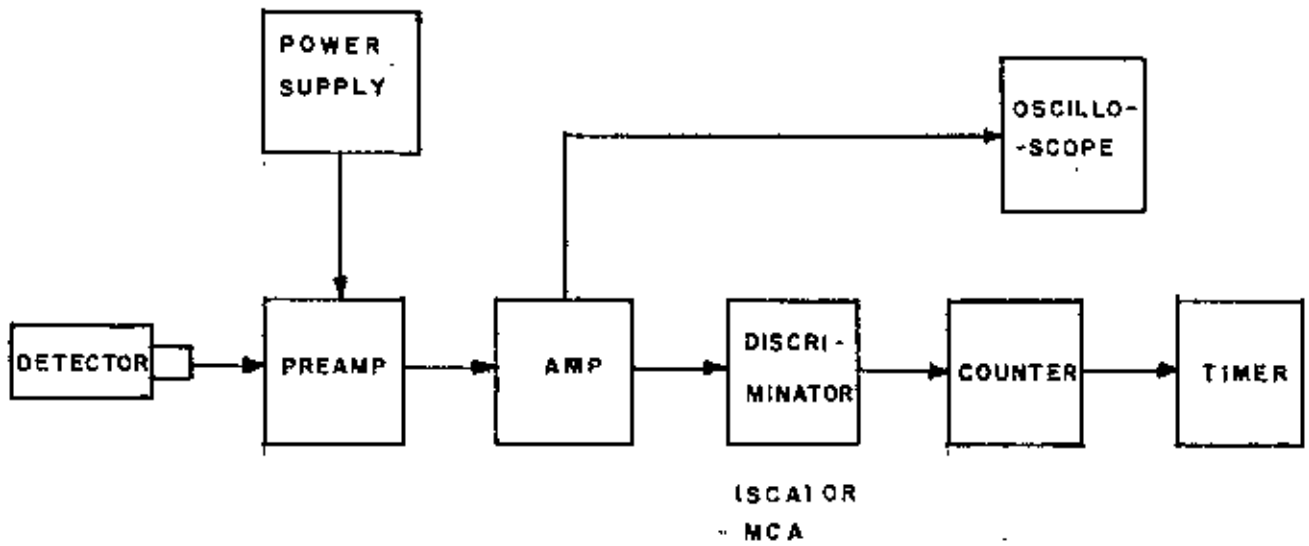
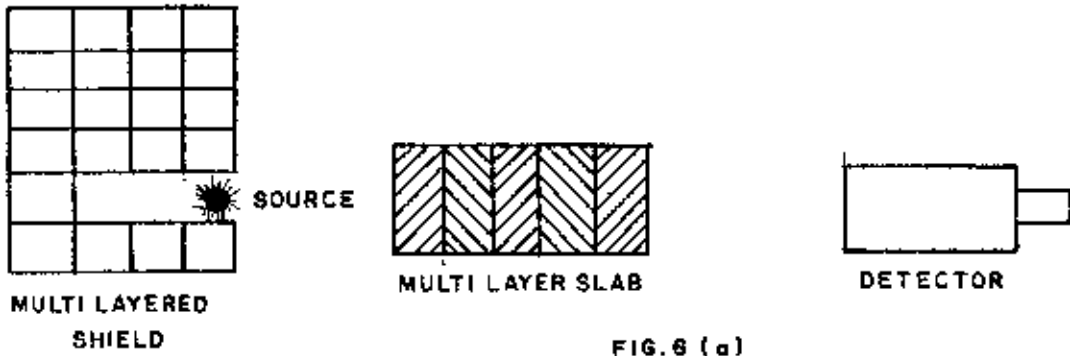


Fig. 6(a) A BLOCK DIAGRAM OF EXPERIMENTAL SETUP AND
(b) ELEMENTS OF A TYPICAL SIGNAL CHAIN FOR PULSE COUNTING

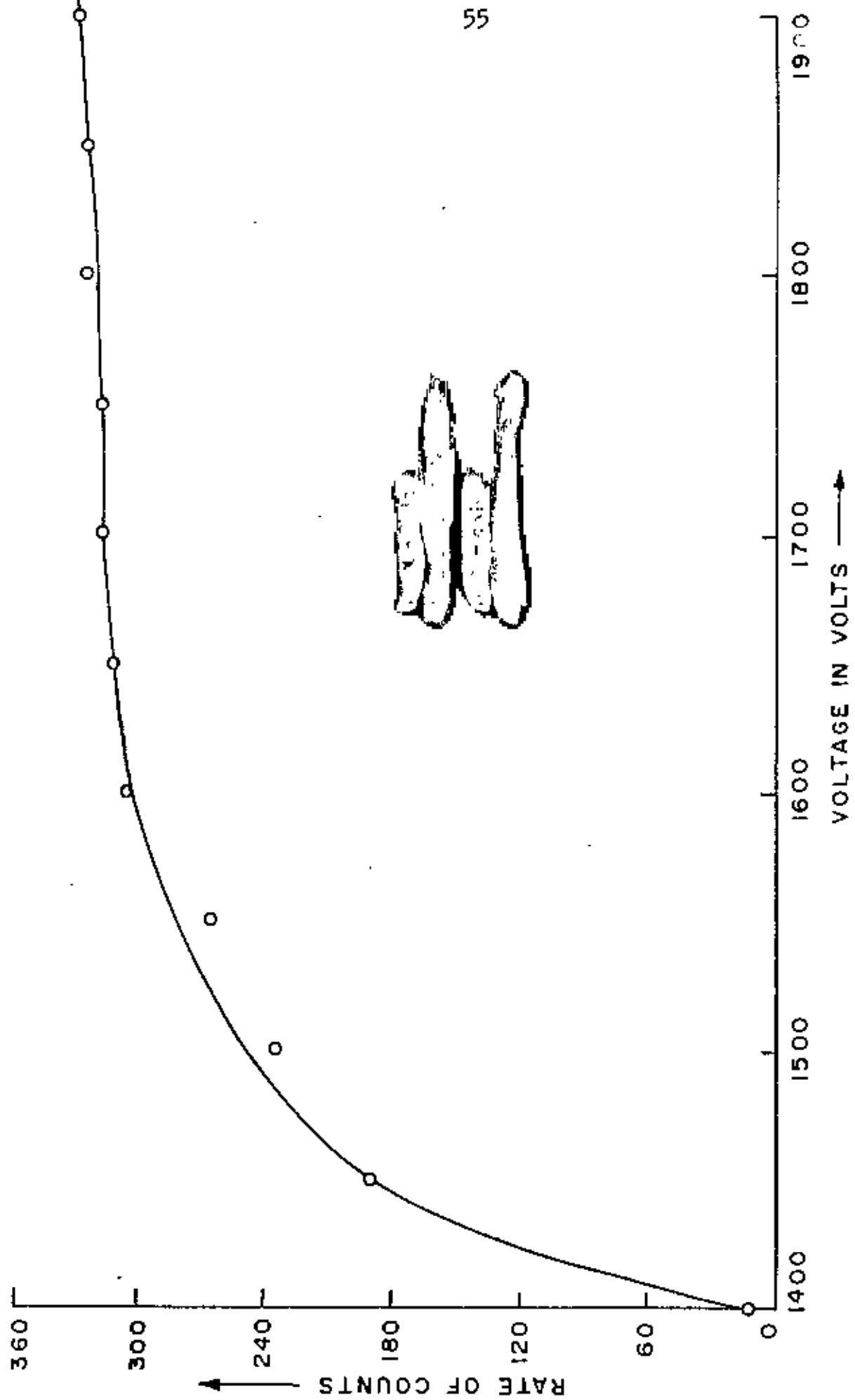


Fig. 7. COUNT RATE VERSUS ANODE VOLTAGE CURVE

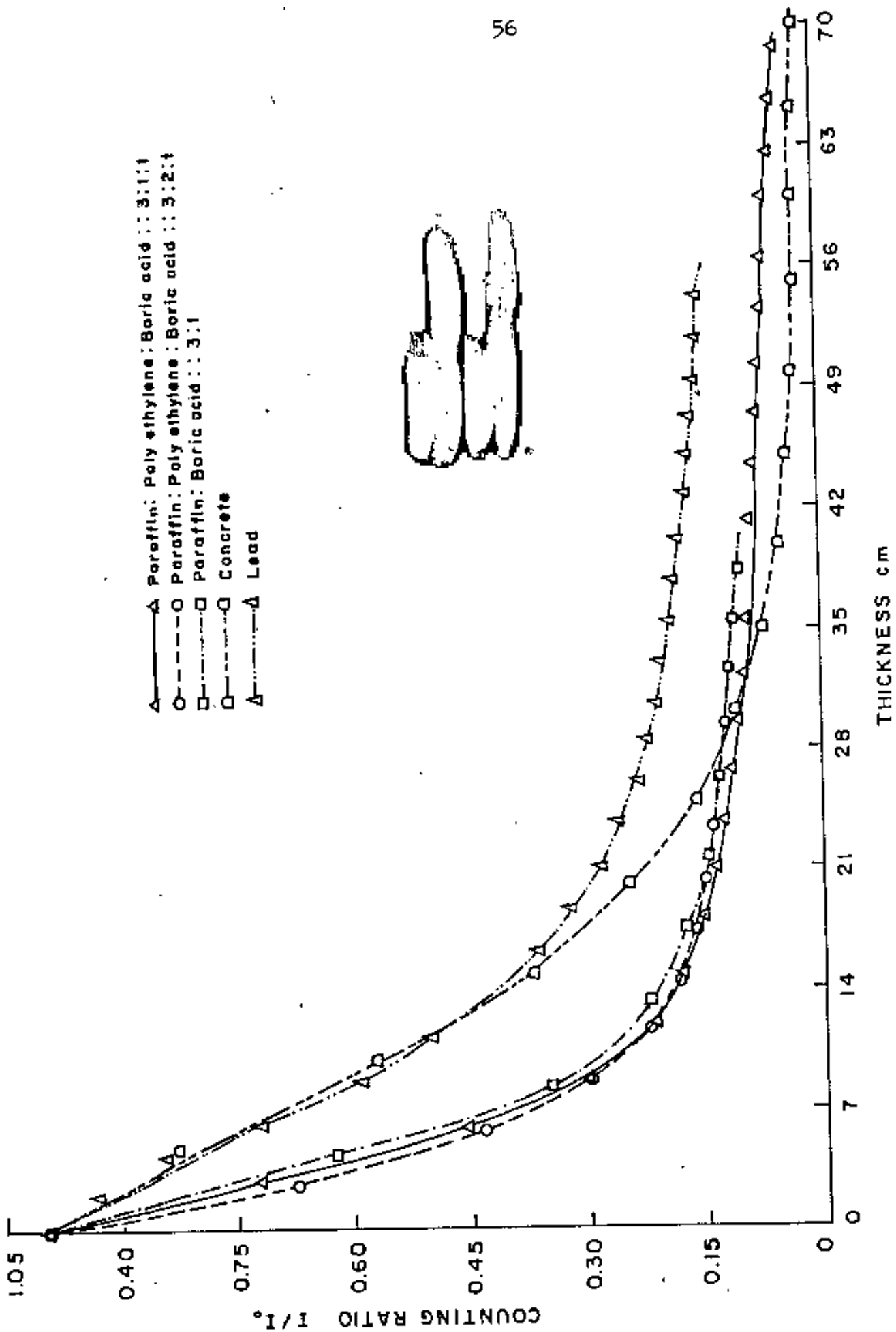


FIG. 8. THE NEUTRON ATTENUATION CURVES

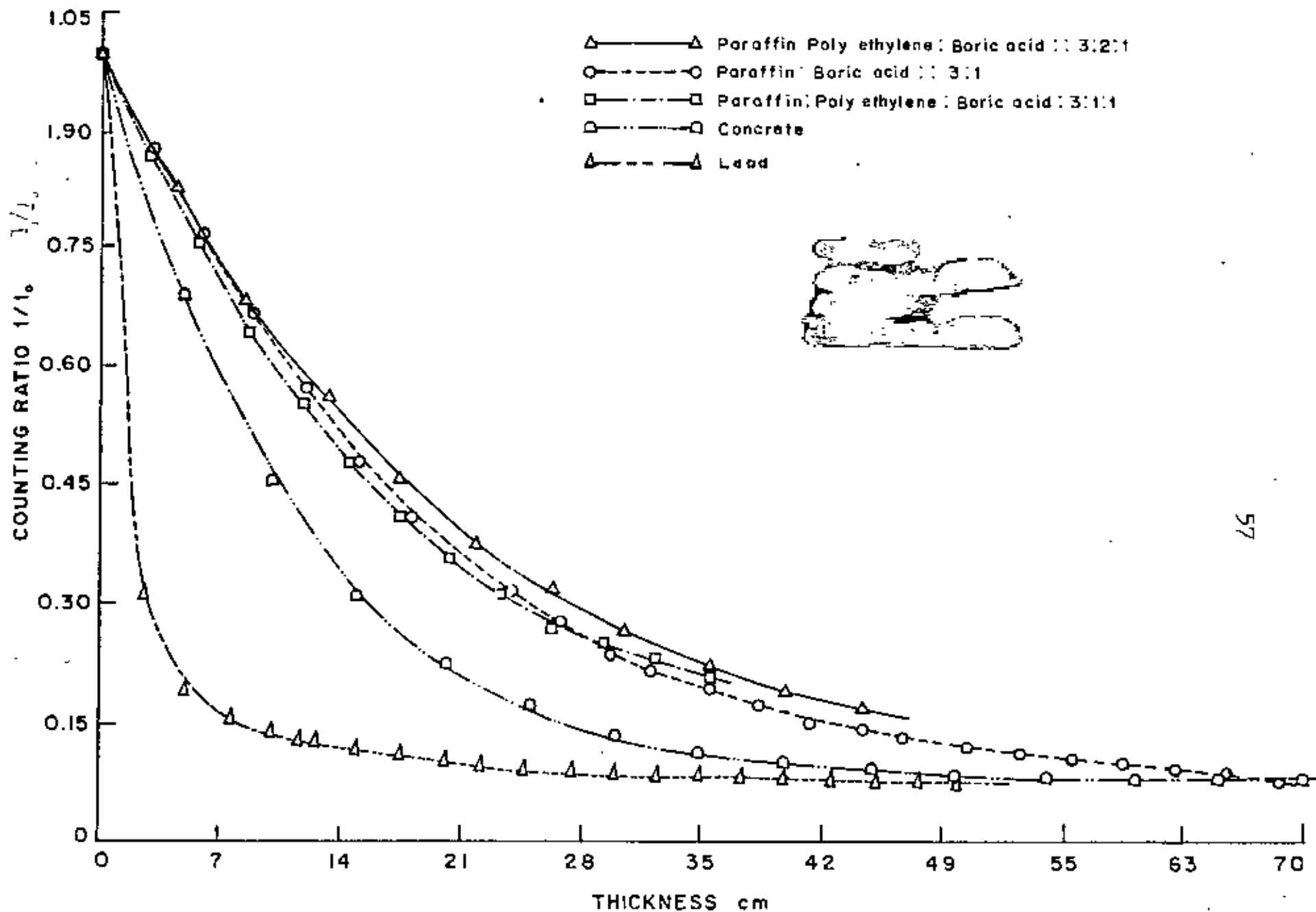


Fig. 9. THE GAMMA-RAY ATTENUATION CURVES

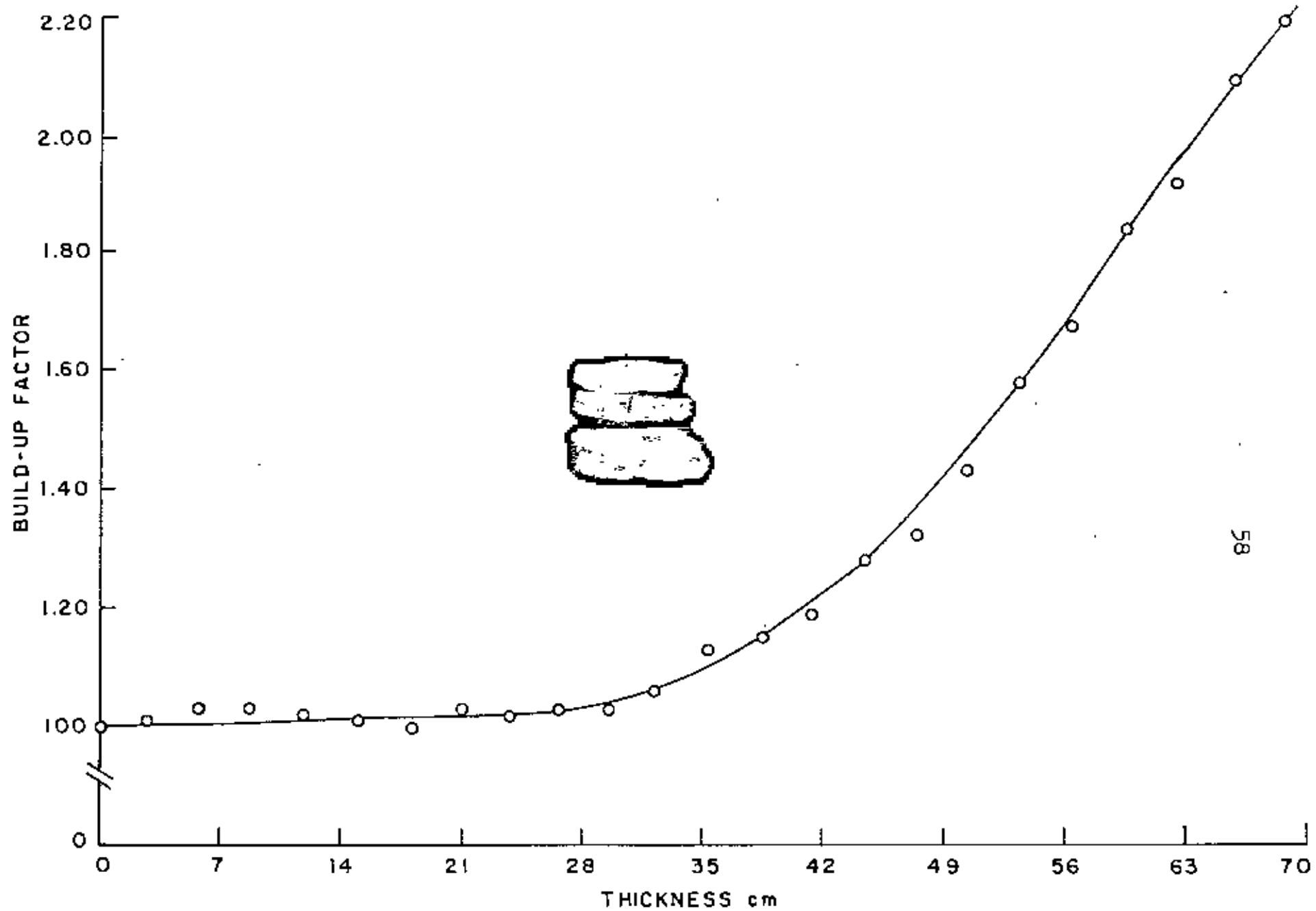


Fig. 10. THE BUILD-UP FACTOR VS THICKNESS CURVE FOR ST. 1.

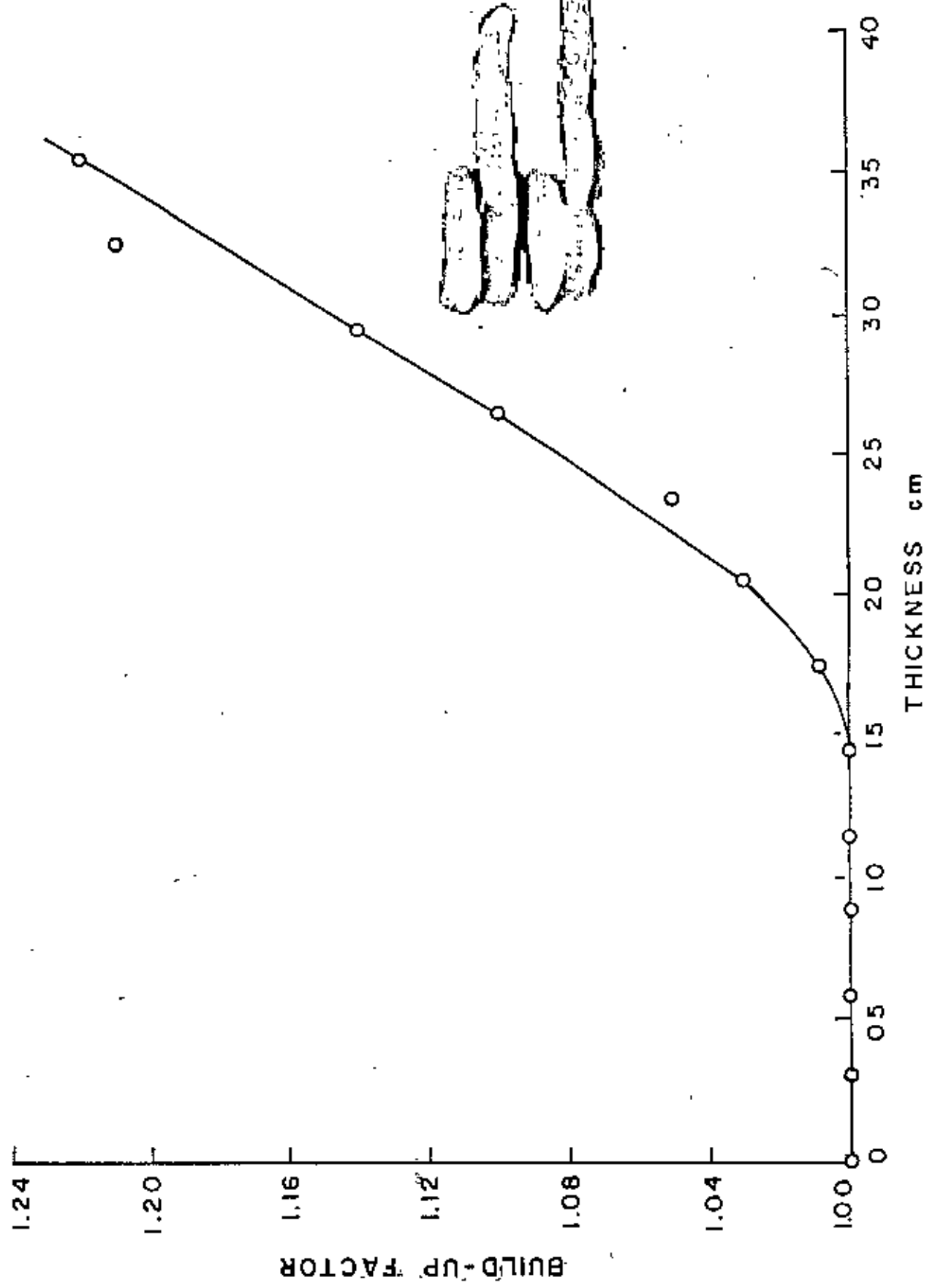


Fig. 11. THE BUILD-UP FACTOR VS THICKNESS CURVE FOR ST 2

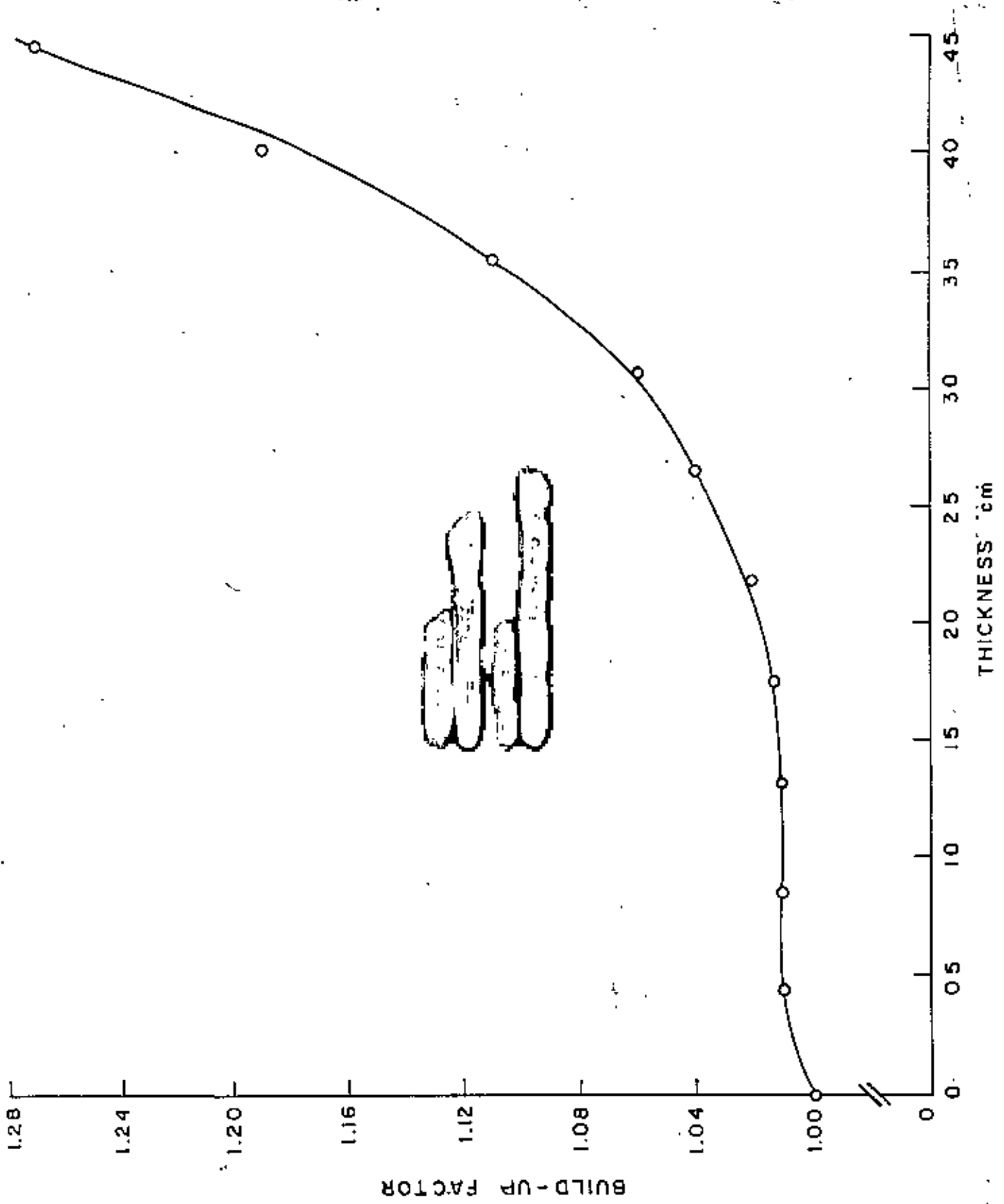


Fig. 12. THE BUILD-UP FACTOR VS THICKNESS CURVE FOR ST3

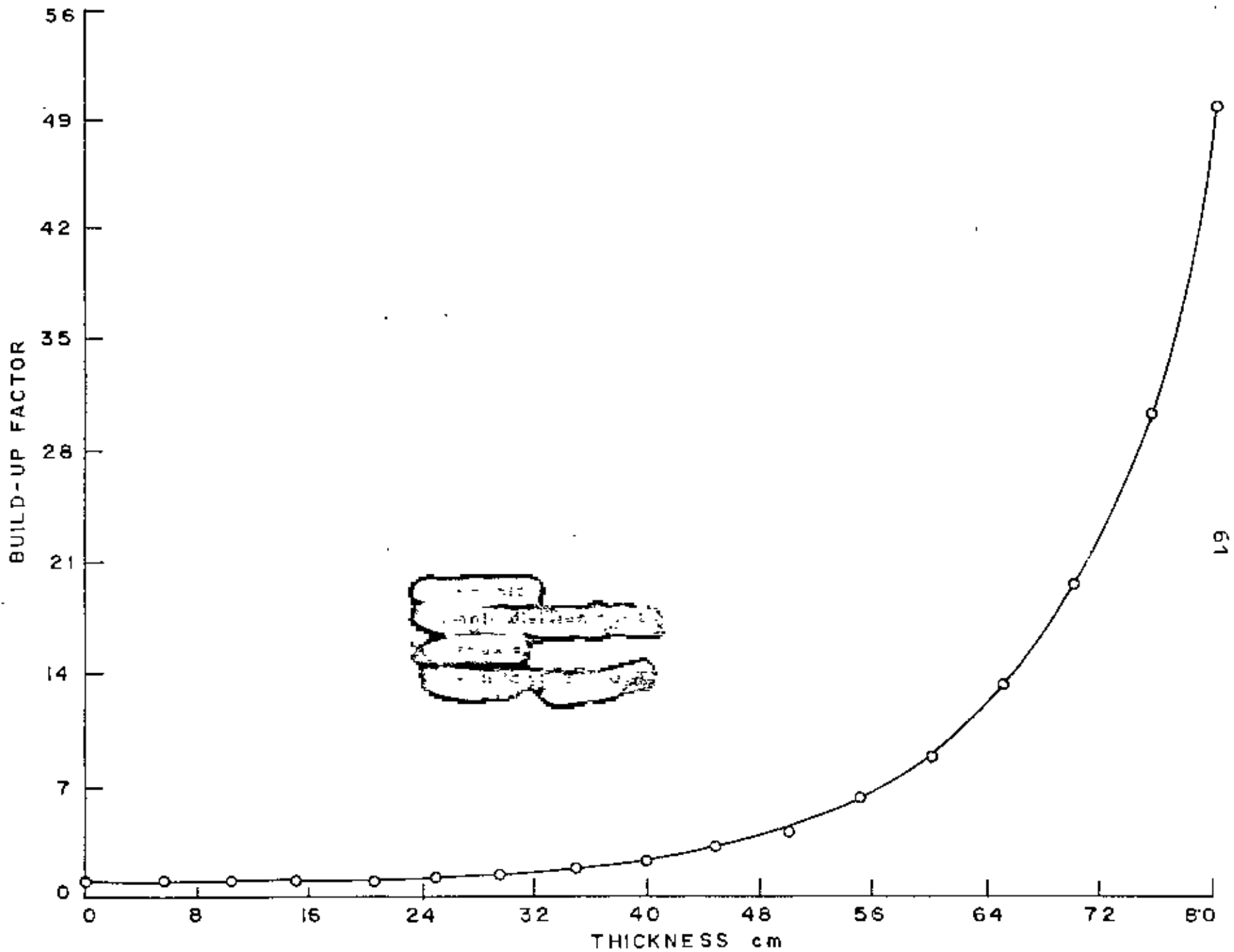


Fig. 13. THE BUILD-UP FACTOR VS THICKNESS CURVE FOR ST 4.

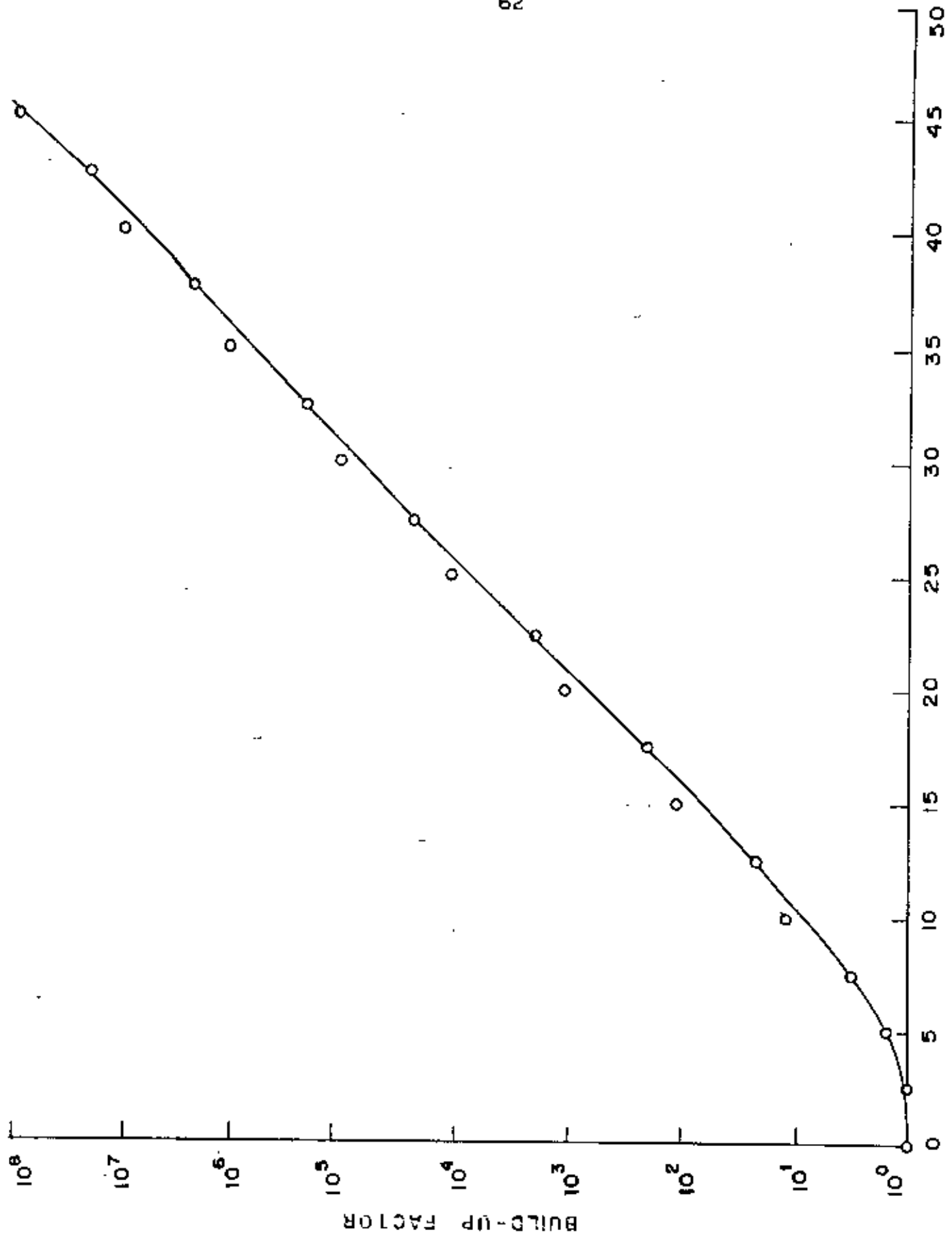


Fig. 14. THE BUILD-UP FACTOR VS THICKNESS CURVE FOR ST5.

CHAPTER 4

OPTIMIZATION OF A MONOCHROMATOR CRYSTAL

4.1 INTRODUCTION

The aim of the present calculations is to design a double axis neutron spectrometer at TRIGA Mark II research reactor of Atomic Energy Research and Establishment (AERE), Savar, Dhaka, Bangladesh. Some calculations on Cu-monochromator have been carried out by H.A. Graf⁽⁵⁾ using his computer program MONREF for particular diffractometer geometries. We have calculated the quantitative resolution functions at the sample position for different collimation angles of the soller collimators in front of and behind the Cu (200) monochromator for a geometry of the proposed diffractometer (described in the next section). Optimization of different parameters of the monochromator, for instance, mosaic spread and thickness has also been done. We have found that the optimum parameters of the monochromator are dependent on diffractometer geometries. The integrated intensities at the sample position for necessary range of neutron wavelengths have been calculated for the plane (200) of copper monochromator to provide information about the suitability of the crystal plane for a particular neutron wavelength.

The program MONREF has been modified to calculate the quantitative angle (Full-Width at Half Maximum) and energy resolution at the sample position and intensity distribution over an energy range. The reflectivity of many crystals were previously calculated by using the diffraction theory of G.E. Bacon and R.D. Lowde⁽³⁴⁾. The calculations based on their formula for absorbing mosaic crystal in symmetric transmission or reflection geometry have been carried out

by P. Fischer⁽³⁵⁾ and A.K. Freund^(36,37). In the latter calculations, the beam collimation was not taken into account and hence their calculations were carried out not on the basis of optimum mosaic spread for practical uses of monochromators in the diffractometer.

The present calculations have been done on the basis of beam collimation. The results presented here will meet up the purpose of selecting the Cu-monochromator and the angular divergence of soller collimators in front of and behind the monochromator of the diffractometer. It will also provide the information about the behaviour of resolutions as a function of mosaicity of the crystal. The experimenters will use these results for designing the experimental set ups for their required resolutions. Some computer results on Cu(200) monochromator crystal using modified MONREF program for a particular geometry are given in Appendix .

4.2 DIFFRACTOMETER GEOMETRY

A block diagram of the diffractometer geometry has been shown in Fig. 15. The primary collimator i.e. the inpile collimator is 50mm X 50mm in cross-section and 1530mm in length. The soller collimators in front of and behind the monochromator have both angular divergence of $30'$ ($\alpha_1 = 0'$, $\alpha_2 = 20'$). The convenient distance between monochromator and sample has been chosen as 2000 mm. The diameter of the portion of the beam port of the TRIGA Mark II research reactor from the cylindrical reactor tank to the inpile collimator is 152 mm. The effective entrance window for the neutrons has been shown in Fig. 15.

4.3 THEORY

The detailed description of the formulation of the reflectivity used in the program MONREF has been given by H.A. Graf⁽³⁾. Here it has been very briefly outlined to give an idea for easy understanding of the method of calculations.

The integrated intensity at the sample position is obtained by a two-fold numerical (trapezoidal) integration over all directions β_2 (deviations of the scattered neutrons from the central line of the sample to the monochromator) and wavelengths λ at the sample position.

$$I_s = \int_{\beta_{2 \min}}^{\beta_{2 \max}} T(\beta_2) d\beta_2 \int_{\lambda_{\min}(\beta_2)}^{\lambda_{\max}(\beta_2)} I_s(\lambda) T(\beta_1) R^n d\lambda. \quad (1)$$

In equation (1) $T(\beta_1)$ and $T(\beta_2)$ are the weighting factors for soller collimators in front of and behind the monochromator respectively:

$$T(\beta_1) = \exp [-(\beta_1/\alpha_1')^2] \quad (2a)$$

$$T(\beta_2) = \exp [-(\beta_2/\alpha_2')^2] \quad (2b)$$

The parameter α' is related to the geometrical divergence α of a soller collimator as follows:

$$\alpha' = \frac{\alpha}{[2 \ln(2)]^{1/2}} \quad (2c)$$

$I_0(\lambda)$ is the intensity of neutrons of wavelength λ at the entrance window.

In this calculation $I_0(\lambda)$ is taken to be 1 for all wavelengths. The parameter R^n (n for normalized power) is related to the total reflectivity R^T (T for total power),

$$R^n = R^T \frac{Q_i}{Q_r} \quad (3)$$

where Q_i and Q_r are the spatial cross-sections of incident and reflected beams of parallel neutrons respectively. The reflectivity R^T is given by

$$R^T = \frac{P_d^t(0)}{P_i^t(0)} \quad (4)$$

where P_i^t is the total power of the incident parallel beam of neutrons at the depth $t = 0$ of the crystal and $P_d^t(0)$ is the total power of the diffracted beam of parallel neutrons at the depth $t=0$ of the crystal in unit of neutrons per sec.

In these calculations, the flux density Φ_s at the sample position has been derived from the reflectivity of the monochromator, the solid angle Ω subtended at the entrance window by the aperture at the sample position and the flux density Φ_0 at the entrance window:

$$\Phi_s = R_i^\lambda \cdot \Omega \cdot \frac{\Phi_0}{4\pi} \cdot \frac{2}{\lambda} \left(\frac{E}{kT}\right)^2 \exp\left(\frac{-E}{kT}\right) \quad (5)$$

where R_i^λ is the integrated intensity (in Å) of a fixed crystal in a perfectly collimated beam of white radiation, k is the Boltzmann constant and T is the temperature in Kelvin. Other symbols have their usual meanings. This is described in detail by G.E. Bacon⁽³⁸⁾. The total integrated intensity as calculated in MONREF is related to R_i^λ as follows:

$$I_s = R_i^\lambda \cdot \alpha_p = \partial_\lambda \cdot \alpha_h \quad (6)$$

where α_h is the horizontal angle over which the entrance window is seen from the sample position and ∂_λ is the wavelength range in the incident beam over which diffraction is complete. Using the Maxwell distribution factor D_{MAXWELL} , flux density at the sample position is given by

$$\Phi_s = I_s \cdot \alpha_v \cdot (\Phi_0/4\pi) \cdot D_{\text{MAXWELL}} \quad (7)$$

where α_v is the vertical angle over which the entrance window is seen from the sample and D_{MAXWELL} is given by

$$D_{\text{MAXWELL}} = 2 \left(\frac{E}{kT}\right)^2 \exp\left(\frac{-E}{kT}\right) / \lambda$$

$$D_{\text{MAXWELL}} = 2 \left(-\frac{\lambda_T}{\lambda} \right)^4 \cdot \exp \left(-\frac{\lambda_T^2}{\lambda^2} \right) / \lambda \quad (8)$$

The factor D_{MAXWELL} calculated for $\lambda_T = 1.74 \text{ \AA}$ corresponding to the moderator temperature of 313°K of the TRIGA Mark II research reactor at 3MW power level is shown as a function of λ in Fig. 16.

4.4 RESULTS AND DISCUSSIONS

The calculations may be divided into two sets: In the first set the crystal thickness and mosaic spreads were optimized. In the second set of calculations, the collimation looking at the resolutions and integrated intensities at the sample position were optimized. Results of the first set of calculations are plotted in three types of curves which include variation of integrated intensity at the sample position with (i) variation of mosaic spread, (ii) variation of monochromator thickness and (iii) variation of neutron wavelength. All the calculations were done taking the geometry of Fig. 15. It may be mentioned that the integrated intensity at the sample position is very much dependent on the diffractometer geometry and collimation of the neutron beam.

The integrated intensities at sample position for different thickness and for different mosaic spread are given in Table 17 for a particular wavelength ($\lambda = 0.6 \text{ \AA}$) and the integrated intensities at sample position for different thickness and for different

wavelength are given in Table 18 for a particular mosaic spread 20 minute.

Table 19 shows results of the present study and that of Graf⁵ with extinction factors of 1.0. In this table, 'O' refers to the present calculations and 'H' to those of reference 5. The distance from monochromator to entrance window of the neutrons was 372.9 cm in the present calculation and 466.0 cm for that of Graf. The collimators for these two cases were different. In our calculations, we used soller collimators before and behind the monochromator while Graf did not use the soller collimators in these positions. At sample position the neutron beam divergence was $1/2^\circ$ for both cases. These two results show a large difference in integrated intensities at sample position. Also due to the difference in collimators, the optimum parameters of the monochromators have been found different. The integrated intensity at sample position for the present case was about three times less than that of Graf's case for all wavelengths and mosaic spreads except for wavelength of 0.6 Å.

Three types of curves which include variation of integrated intensity at sample position with (i) variation of mosaic spread, (ii) variation of monochromator thickness and (iii) variation of neutron wavelength have been plotted of which only a few representative ones are shown. Fig. 17 shows the variation of integrated intensity at the sample position with variation of mosaic spread for different crystal thickness. The optimum mosaic

spread can be found for a particular crystal thickness from these curves. Fig. 18 give integrated intensities at sample position with respect to variation of crystal thickness for different mosaic spreads. These curves give the optimum thickness of a crystal for a particular mosaic spread. The third set of curves, shown in Fig. 19, are the plots of integrated intensities at the sample position with respect to variation of λ for optimum mosaic spreads. These curves show the limitations of choosing λ for a plane of the Cu crystal. The integrated intensity is always increasing with increasing mosaic spread upto a certain limit despite the inverse behaviour of the peak reflectivity. The calculations show that the thick crystal with small mosaic spread has higher reflectivity than a thin one with large mosaic spread.

In the present calculations, the integrated intensity at sample position is in units of $\text{rad} - \text{\AA}$, but one can easily calculate the flux density at sample position in units of $\text{n-cm}^{-2} \text{ sec}^{-1}$ by using equation (7), where D_{MAXWELL} is found from Fig. 16. The above discussions make it clear that for the particular diffractometer geometry of the present case, these calculations are very useful for designing the diffractometer and choosing the optimum size of the Cu monochromator.

Table 17: Integrated intensities at sample position for different thickness and for different mosaic spread

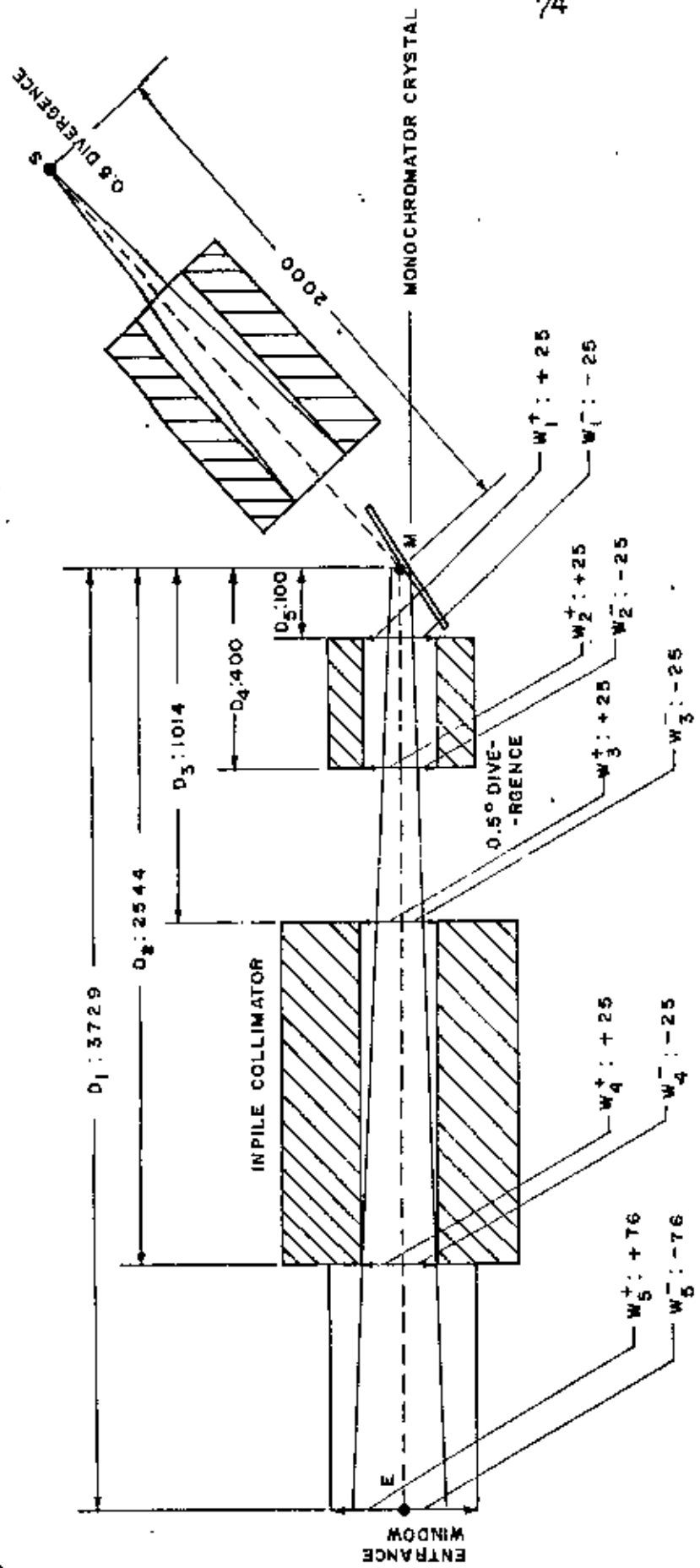
Soller Colli- mators $\alpha_1 \alpha_2$	Cry- stal plane	Primary extinc- tion	Wave- length (A)	Thick- ness (mm)	Integrated intensities $I_i(t)$ for mosaic spread									
					5	10	15	20	25	30	35	40	45	
				1	0.14079	0.16520	0.16880	0.16386	0.15469	0.14407	0.13355	0.12381	0.11462	
				2	0.16575	0.20622	0.21705	0.21441	0.20479	0.19235	0.17950	0.16730	0.15558	
				3	0.17132	0.21732	0.23147	0.23042	0.22130	0.20874	0.19545	0.18269	0.17031	
0 20	Cu200	1.00	0.6	4	0.17275	0.22049	0.23590	0.23558	0.22679	0.21434	0.20102	0.18815	0.17562	
				5	0.17316	0.22144	0.23730	0.23726	0.22863	0.21626	0.20296	0.19015	0.17754	
				6	0.17329	0.22174	0.23775	0.23782	0.22926	0.21692	0.20365	0.19079	0.17823	
				7	0.17334	0.22184	0.23789	0.23800	0.22947	0.21715	0.20389	0.19104	0.17848	
				8	0.17335	0.22187	0.23794	0.23806	0.22954	0.21723	0.20397	0.19112	0.17857	
				9	0.17336	0.22188	0.23796	0.23809	0.22956	0.21726	0.20400	0.19116	0.17861	
				10	0.17336	0.22189	0.23797	0.23809	0.22957	0.21727	0.20401	0.19117	0.17862	
				11	0.17336	0.22189	0.23797	0.23810	0.22958	0.21727	0.20402	0.19117	0.17862	
				12	0.17336	0.22189	0.23797	0.23810	0.22958	0.21727	0.20402	0.19117	0.17863	

Table 18: Integrated intensities at sample position for different thickness and for different wavelength for a particular mosaic spread.

Soller Colli- (mix) $\alpha_1 \alpha_2$	Crv- stal plane	Mosaic spread (mm)	Pri- mary extinc- -tion	Thick- ness (mm)	Integrated intensities $I_s(t)$ for wavelengths Rad. $\text{\AA} \times 10^{-1}$				
					=0.6 \AA	=1.2 \AA	=1.6 \AA	=2.0 \AA	=2.4 \AA
				1	0.16880	0.33788	0.41973	0.47658	0.558
				2	0.21705	0.46099	0.54985	0.61134	0.677
				3	0.23147	0.51073	0.60097	0.66436	0.720
				4	0.23590	0.53189	0.62334	0.68827	0.737
0 20	Cu 200 20		1.00	5	0.23730	0.54123	0.63389	0.70010	0.745
				6	0.23775	0.54549	0.63919	0.70638	0.751
				7	0.23789	0.54749	0.64200	0.70993	0.755
				8	0.23794	0.54846	0.64356	0.71203	0.757
				9	0.23796	0.54895	0.64446	0.71332	0.758
				10	0.23797	0.549199	0.64499	0.71414	0.759
				11	0.23797	0.54932	0.64532	0.71467	0.759
				12	0.23797	0.54939	0.64552	0.71502	0.760

Table 19: Integrated intensity $I_f(t_{\infty})$ for large crystal thickness and $I_s(t)$ for a crystal thickness of 6 mm for primary extinction 1.00, for Cu monochromators. I_f is given in units of ($\times 10^{-4}$ rad. \AA^2)

Optimum mosaic spread		Wavelength	Crystal Plane	Cu 200	Optimum mosaic spread	Crystal plane Cu 200
		λ				
(O)	(H)	\AA	(O)	(H)	(F)	(F)
15'	25'	0.6	$I_f(t_{\infty})$: 0.238	0.270	15'	-
			$I_s(t)$: 0.238	0.270		-
20'	25'	1.2	$I_f(t_{\infty})$: 0.550	1.66	20'	0.510
			$I_s(t)$: 0.545	1.61		0.500
20'	25'	1.6	$I_f(t_{\infty})$: 0.646	2.11	20'	0.620
			$I_s(t)$: 0.640	2.02		0.610
20'	25'	2.0	$I_f(t_{\infty})$: 0.715	2.31	20'	0.660
			$I_s(t)$: 0.0706	2.21		0.650
20'	25'	2.4	$I_f(t_{\infty})$: 0.760	-	20'	0.640
			$I_s(t)$: 0.751	-		0.630



ALL DIMENSIONS ARE IN MILLIMETRES

Fig. 15. A BLOCK DIAGRAM OF THE DIFFRACTOMETER GEOMETRY

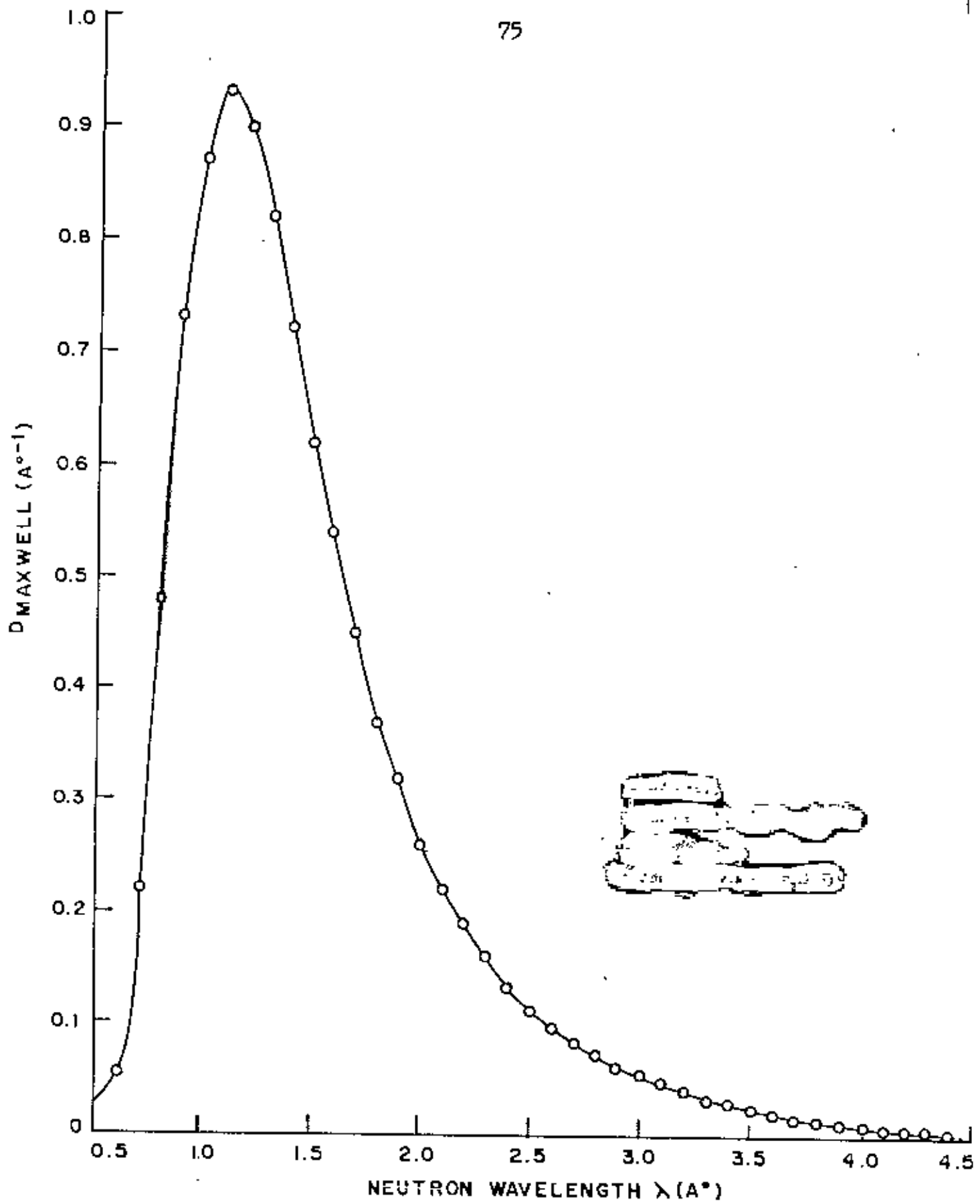


Fig. 16. MAXWELL DISTRIBUTION FACTOR FOR TRIGA MARK II REACTOR AT AERE, DHAKA AT 3MW POWER LEVEL

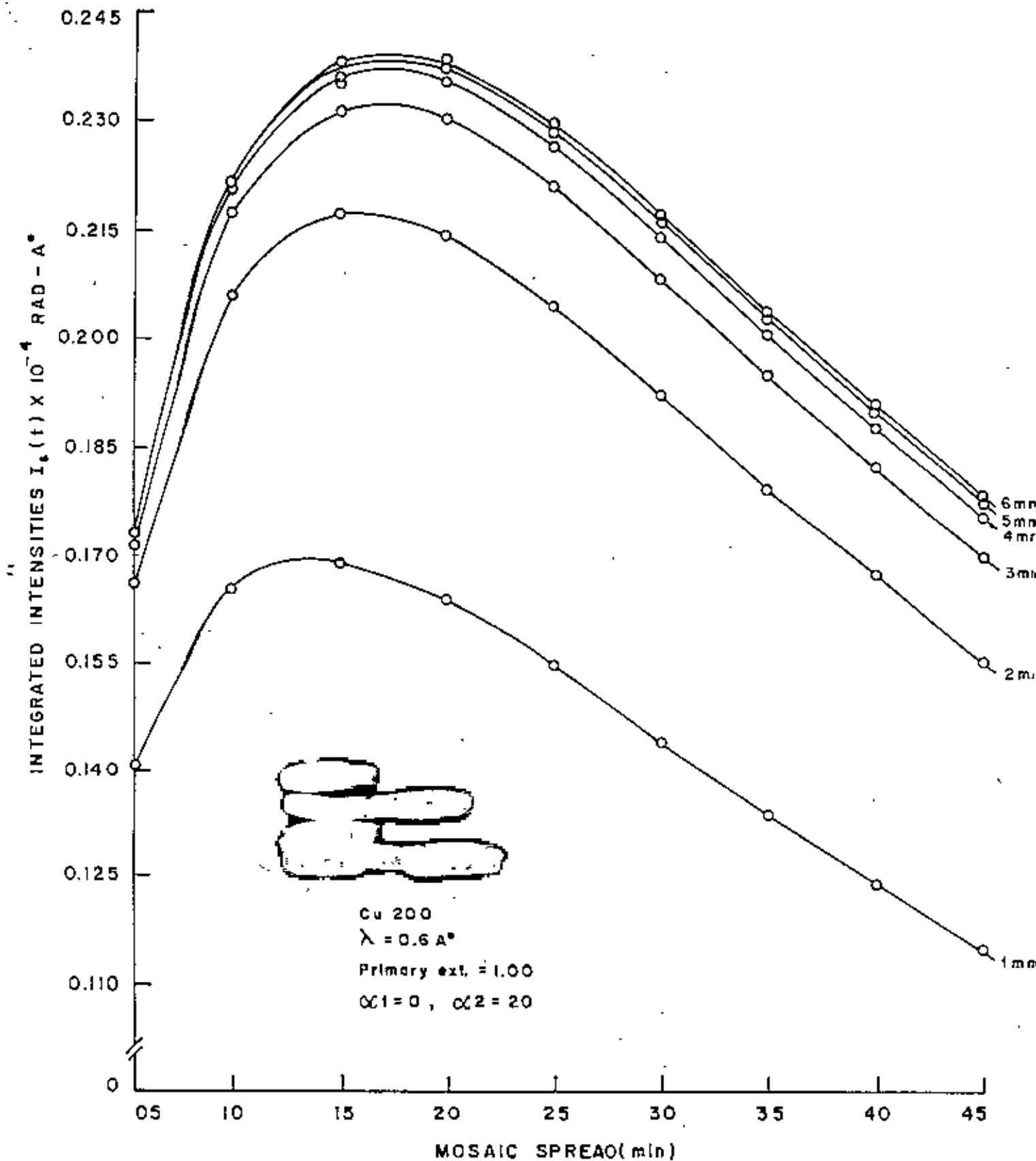


Fig. 17. THE VARIATION OF INTEGRATED INTENSITY AT SAMPLE POSITION AS A FUNCTION OF MOSAIC SPREAD (min)

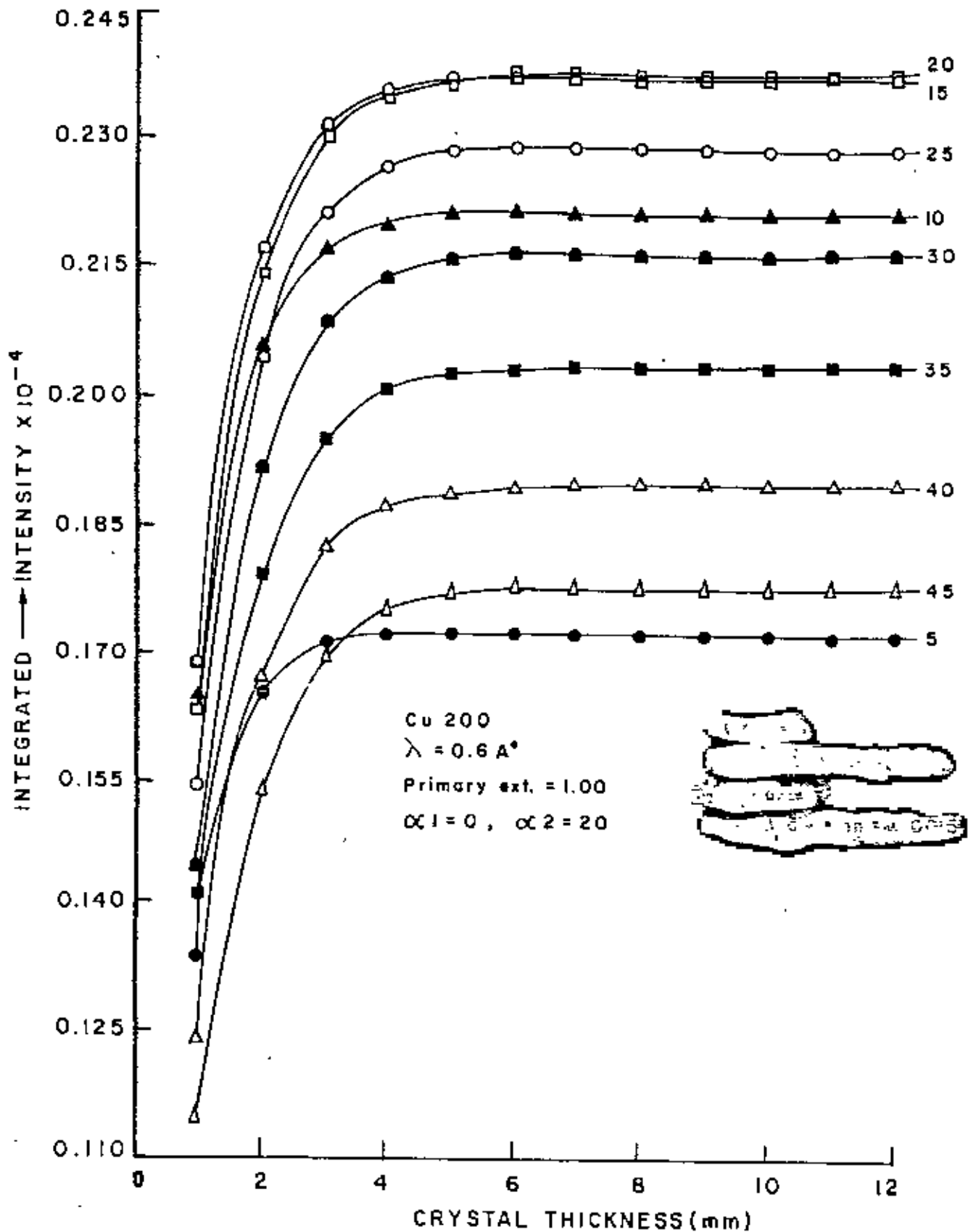


Fig. 18. THE VARIATION OF INTEGRATED INTENSITY AT SAMPLE POSITION AS A FUNCTION OF CRYSTAL THICKNESS (mm)

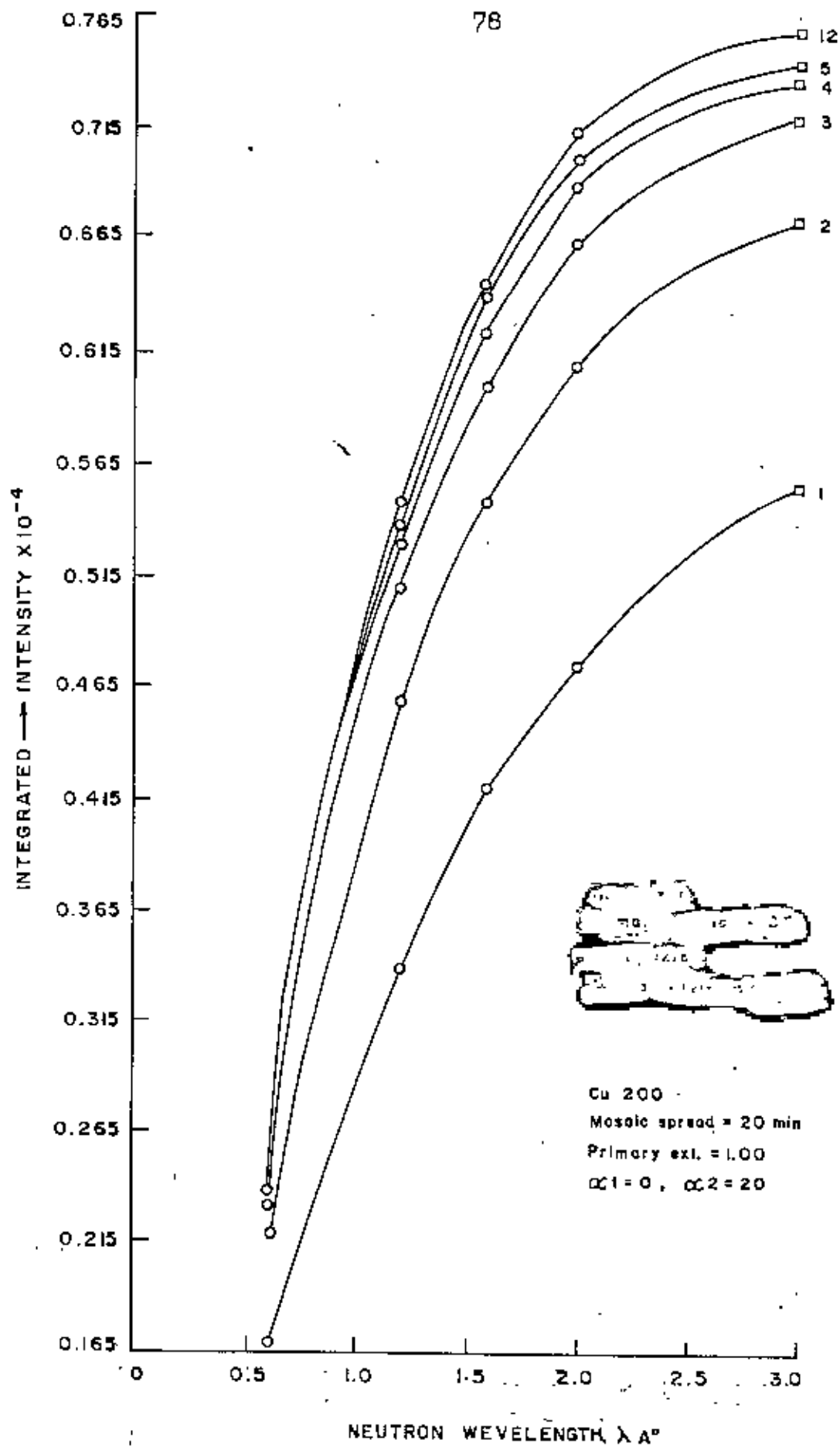


Fig. 19. THE VARIATION OF INTEGRATED INTENSITY AT SAMPLE POSITION AS A FUNCTION OF THE NEUTRON WAVELENGTH.

CHAPTER 5
CONCLUSIONS

CONCLUSIONS

A beam of neutrons from a collimating tube in the reactor falls on to a monochromating crystal which is surrounded by a massive shield attached to the reactor face. Shielding of this sort is essential for protecting both the operator and the detecting apparatus from the main beam of neutrons and gamma-rays emerging from the collimator. Only about 1 percent of this mixed radiation, namely thermal neutrons having wavelengths within a narrow band is reflected by the monochromator and used in the subsequent neutron diffraction measurements. Many of the scattered neutrons would enter the counter and give a large background count against which it will be very difficult to distinguish the diffracted neutron beams. The fast neutrons are slowed down by collision with the hydrogen atoms in the borated paraffin shield and subsequently absorbed by the boron which has a high absorption cross-section for slow neutrons. On the other hand, the gamma-rays are absorbed by the lead screen. An effective system of shielding is important not only to reduce the background of scattered neutrons which would be picked by the counter but also to ensure that the general level of radiation in the neighbourhood is sufficiently low from health and safety points of view⁽³⁹⁾. The main objective of the present investigations is to develop technical know how for design and fabrication of a monochromator drum of a double-axis neutron spectrometer.

The results on the shielding effectiveness for neutron suggest that

the shielding materials ST1 and ST2 have a higher neutron removal cross-section than other shielding materials under investigation. For a small thickness of the shielding material, ST2 shows more attenuation effect than ST1 and for large thickness, ST1 gives more attenuation effect than ST2. It is concluded that adding more polyethylene causes higher neutron attenuation effect for small thickness.

The results on the shielding effectiveness for gamma rays show that shielding material ST5 has greater gamma-ray attenuation effect than the others. It is observed that higher value of gamma-ray attenuation co-efficient arises due to the higher density of the material. It has already been mentioned that gamma-ray attenuation co-efficients and relaxation lengths for ST5 and ST4 are better than those of ST1, ST2 and ST3. From Table 16, it is seen that shielding material ST5 and ST4 have smaller relaxation lengths than ST1, ST2 and ST3. This suggests that ST5 and ST4 have more scattering centres and obviously the build-up factors are higher for ST5 and ST4 due to the multiple scattering than those of others.

From the above discussions, it may be concluded that shielding materials ST5 and ST4 are more effective than ST1, ST2 and ST3 for gamma-ray shielding measurements. It is mentioned that ST5 is more effective than ST4. For neutron shielding measurements, shielding materials ST1, and ST2 are more effective than those of ST4 and ST5. So, in designing of the monochromator drum shielding

arrangement, the monochromator drum requires 18 cm of lead i.e. ST5 (for gamma ray) 50 cm of borated paraffin i.e. ST1 and ST2 (for slowing down of fast neutrons and subsequent capture), 1.5 cm of stainless steel (for epithermal and fast neutron partly) and 20 cm of I-M concrete i.e. ST4 (for gamma-rays and neutron radiations).

The comparative studies of the shielding materials polyboron^(18,20) and borated paraffin are as follows: The ratios of the components of the presently prepared borated paraffin are paraffin wax: polyethylene : boric acid :: 3:2:1. This material is called in the text as ST2. As can be seen from Table 16, the gamma-ray attenuation co-efficients and neutron removal cross-sections are approximately same for both the materials. The relaxation length of polyboron for gamma-rays is slightly higher than that of ST2. But the relaxation length of polyboron for neutrons is slightly smaller than that of ST2. This small variation in relaxation length does not make any significant difference. Therefore, it may be concluded that the shielding material used in the present experiment will suffice and moreover, it will be cheaper than polyboron.

The integrated intensity at sample position is very much dependent on diffractometer geometry and collimation of the neutron beam. The results of the present study show that the optimum parameters of the monochromators have been found different due to the difference in collimations (compared with Graf's case). The integrated intensity at sample position for the present case was about three times greater than that in Graf's case for all wavelengths and

mosaic spreads except for the wavelength 0.6Å. It is clear that for designing the diffractometer and choosing the optimum size of the Cu monochromator for a particular diffractometer geometry, these calculations are very useful. The calculations show that the thick crystal with small mosaic spread has higher reflectivity than a thin one with large mosaic spread.

Finally, it is concluded that knowledge about monochromator design and optimization of monochromator crystal will be helpful in designing a two-axis neutron spectrometer at the 3MW TRIGA Mark-II research reactor at AERE, BAEC, Savar, Dhaka, Bangladesh.

REFERENCES

1. ELSASSER, W.M. C.R. Acad. Sci. Paris, 202, 1029, 1936.
2. HALBAN, H. and PREISWERK, P.C.R. Acad. Sci. Paris, 203, 73, 1936.
3. MITCHELL, D.P. and POWERS, P.N. Phys. Rev. 50, 486, 1936.
4. ZINN, W.H. Ibid. 71, 752. 1947. *
5. GRAF, H.A. Hahn-Meitner-Institute für Kernforschung, Berlin GmbH, HMI-B 403, 1983.
6. AHMED, F.U. et al. INST, Internal Report No. INST. 28, RNPD-2, June, 1988.
7. AHMED, F.U., KHAN, A.A., AHSAN, M.H., AWAL, M.A. and AHMAD, A.A.Z. Submitted for publication in the journal of Bangladesh Academy of Sciences.
8. IYENGER. P.K. Thermal Neutron Scattering, Ed. P.A. Egelstaff, Academic Press, London and NewYork, P102, 1965.
9. MACALPIN, W. Nucl. Instr. and Meth. 25, 205, 1965.
10. SOLLER, W. Phys. Rev. 24, 158, 1924.
11. SAILOR, V.L.; FOOTE, H.L, LANDON, H.H; and WOOD, R.E. Rev. Sci. Instr. 27, 26, 1956.
12. CAGLIOTI, G. PAOLETTI, A; and RICCI, F.P. Nucl. Instr. 3, 223, 1958.
13. MOLLAH. A.S; AHMAD, G.U. and HUSSAIN, S.R. Attenuating properties of boron loaded ordinary concrete for neutrons and gamma rays from Californium-252. Submitted for publication in BUET studies.

14. PRICE, B.T.; HORTON, C.C. and SPINNEY, K.T.; Radiation shielding, Pergamon Press, UK, 1957.
15. DUBROVSKI, S., et al. *Kernenergie*, 16, 378, 1973.
16. ADAMS, R.J. and LOKAN, K.H., Proc. conf. on nuclear cross-sections, NBS special publications 425, vol. 1, 409, 1975.
17. ADAMS, R.J. and LOKAN, K.H. *Health Phys.*, 36, 671, 1979.
18. AHMED, F.U. et al. Measurement of gamma-ray shielding properties of I.M. concrete and Polyboron slabs using Cf-252. Submitted for publication in *Nucl. Sci. Engg.*
19. MAKARIOUS, A.S. et al. *Appl. Radiat. Isot.* 40, 257, 1989.
20. AHSAN, M.; BHUIYAN, S.I., AKHTAR, F., ROUF, M.A. and Hussain, S.R. INST-10, AERE, Dhaka, P.O. Box 3787, 1984.
21. BHUIYAN, S.I. et al. *Health Phy* 57, 1989.
22. AHMED, F.U. et. al. *Nucl. Sci Engg.* 85, 427, 1983.
23. GUJRATHI, S.C. and D'AURIA, J.M., *Nucl. Instr. and Meth.*, 100, 445, 1972.
24. UWAMINO, Y. et al. *Nucl. Sci. Engg.* 80, 360, 1980.
25. SENFFLE, F.E. and PHILBJN, P. *Health Phys.* 23, 532, 1972.
26. GLASSTONE, S. and SEASONSKE, A. *Nuclear Reactor Engineering*, Van Nostrand Co., Princeton, N.J. 1967.
27. KUSPA, J.P. and TSOULFANIDIS, N., *Nucl. Sci. Engg.* 52, 117, 1973.
28. HANSON, A.O. and McKIBBEN, M.L., *Phys. Rev.* 72, 673, 1947.
29. McTAGGART, M.H., AWRE NR/AI/59, 1958.
30. EAST, L.V. and WALTON, R.B., *Nucl. Instr. and Meth.* 75, 231, 1969.
31. KNOLL, G.F. *Radiation Detection and measurement*, John Wiley

- and Sons, Inc. USA, 1972.
32. GOLDSTEIN, H. Fundamental aspects of Radiation Shielding Pergamon Press, U.K. 1956.
 33. IAEA Technical Report Series No. 159, Vienna, 1974.
 34. BACON, G.E. and LOWDE, R.D., Acta Cryst, 1, 303, 1948.
 35. FISCHER, P. Report AF-SSP-10, Eidg. Institut fur Reaktor forchung 5303; Wurentingen, 1967.
 36. FREUND, A.K., Int. Sci. Report 8OFR. 335, Institut Max Von Lau-Paul Langevin, France, 1980.
 37. FREUND, A.K., Int. Sci Report 8OFR, 40S, Institut Max Van Lau-Paul Langevin, France, 1980.
 38. BACON, G.E. Neutron Diffraction, 3rd edition, Clarendon Press, Oxford, 1975.
 39. CEMBER, H. Introduction to Health Physics, 2nd edition, Pergamon Press, U.K. 1985.

APPENDIX I

=====
 ***CALCULATIONS DONE FOR VARIABLE THICKNESS ***

**CALCULATIONS DONE FOR FIXED COLLIMATION **

=====
 PARAMETERS FOR THE REFLECTIVITY CALCULATIONS
 =====

* CU 200:STANDARD DIFFRACTOMETER CONFIG. WITH DIFF. SOLER COLL**

CRYSTAL TYPE: CU 200

LAMBDA=1.20 ANGSTR. INCIDENT ENERGY.=56.805 MEV PRIM. EXT.=1.00

MOSAIC SPREAD = 20.0 MIN. ALPHA1 = 0.0 MIN. ALPHA2 = 20.0 MIN.

SQUARED SCATTERING LENGTH DENSITY (F/VCELL**2) : 0.3900D+22(1/CM**4)

ZERO WAVE-LENGTH: 1.200 (ANGSTROEM)

ZERO BRAGG ANGLE: 19.387(DEGREES)

ABSORPTION FACTOR: 0.700(1/CM)

CRYSTAL THICKNESS: 1.000(MM)

MOSAICSPREAD(FWHH): 20.000(MINUTES)

PRIM. EXTINCTION: 1.000(1.=NO EXT.)

BETA (=DEVIATION FROM ZERO BRAGG POSITION) : 0.000(DEGREES)

DEL(= ANGLE BETWEEN NET PLANE AND CRYSTAL SURFACE): 0.000(DEGREES)

CLNEG (= LEFT (-PHI2) SIDE LENGTH OF THE MONOCHROMATOR: -50.000(MM.)

LPOS (= RIGHT (+PHI2) SIDE LENGTH OF THE MONOCHROMATOR: 50.000(MM.)

DISTANCE MONOCHROMATOR - SAMPLE: 2000.000 (MM.)

RADIUS OF CURVETURE (ZERO MEANS FLAT MONOCHROMATOR): 0.000(MM).

ALPHA 1 (SOLLER COLLIMATOR 1): 0.000(MINUTES)

ALPHA2 (SOLLER COLLIMATOR 2): 20.000(MINUTES)

PHI2-MIN (0. MEANS USE CALCULATED LIMIT) : -0.500(DEGREES)

PHI2-MAX (0. MEANS USE CALCULATED LIMIT) : 0.500(DEGREES)

LIMIT FOR PHI2-MIN CALCULATED FROM CLNEG: -0.465(DEGREES)

LIMIT FOR PHI2-MIX CALCULATED FROM CLPOS: 0.487(DEGREES)

THE ENTRANCE FLUX F10 : 0.10000D+13 (N.CM-2.S-1)

THE VERTICAL CONVERGENCE -- : 0.0200 RAD

THE GEOMETRICAL LIMITATIONS BETWEEN MONOCHROMATOR
AND CORE (IN MM.)

	DISTANCE FROM	LEFT OPENING	RIGHT OPENING
	MONOCHROMATOR	(-PHI1-SIDE)	(+PHI1-SIDE)
1	100.000	-25.000	25.000
2	410.000	-25.000	25.000
3	1320.000	-25.000	25.000
4	2850.350	-25.000	25.000
5	4034.625	-76.200	76.200

PARAMETERS FOR THE TRAPEZOIDAL INTEGRATION

OVER PHI2:

FROM-0.4645 TO 0.4870 IN 101 STEPS

OVER LAMDA:

ALL WAVELENGTHS SCATTERED WITHIN +/- 3.5 TIMES ETA IN 101 STEPS

(ETA IS THE STANDARD DEVIATION OF THE MOSAIC DISTR.)

VARIABLE PARAMETERS

MOSAIC SPREAD : 20.000(MINUTES)
THICKNESS : 1.000(MM)
RADIUS : 0.000(MM)
WBETA : 0.000(DEGREES)
WDEL : 0.000(DEGREES)

INTENSITY PROFILE OVER PH12 WITH RESPECT TO ANGLE (FACTOR = 0.16254D+05)

-0.600	0.000
-0.550	0.000
-0.500	0.000
-0.450	0.132
-0.400	0.554
-0.350	2.018
-0.300	5.865
-0.250	13.883
-0.200	28.369
-0.150	49.271
-0.100	72.920
-0.050	92.376
0.000	100.000
0.050	92.610
0.100	73.353
0.150	49.352
0.200	28.598
0.250	14.083

0.300	5.719
0.350	2.029
0.400	0.603
0.450	0.148
0.500	0.000
0.550	0.000
0.600	0.000

$K(0) = 5.2360$ (1/ANGSTR.) $K(\text{MIN}) = 5.1544$ (1/ANGSTR.) $K(\text{MAX}) = 5.3$
(INTENSITY PROFILE OVER PHI^2 WITH RESPECT TO ENERGY FACTOR = $0.16280\text{D}+05$)

45.812	1.006
46.911	2.449
48.010	5.731
49.110	11.233
50.110	11.233
50.209	20.219
51.308	33.653
52.408	50.622
53.507	68.788
54.606	85.164
55.706	97.351
56.805	100.000
57.904	93.933
59.004	79.551
60.103	62.593
61.202	44.806
62.302	29.072

63.401	16.613
64.500	8.993
65.600	4.394
66.699	1.938
67.798	0.721
68.898	0.259
69.997	0.083
71.096	0.000
72.196	0.000

THIC(MM) SPHI (RAD*ANG) TPFI (N.CM-2. S-1) ERES(MEV) ARES (DEG) DLAM/ALAM

1.00	0.33788D-04	0.33803D+05	8.51390	0.29711	0.03015
2.00	0.46099D-04	0.46119D+05	8.49703	0.29652	0.03009
3.00	0.51073D-04	0.51096D+05	8.49442	0.29641	0.03008
4.00	0.53189D-04	0.53213D+05	8.49733	0.29650	0.03009
5.00	0.54123D-04	0.54147D+05	8.50175	0.29664	0.03011
6.00	0.54549D-04	0.54573D+05	8.50594	0.29677	0.03012
7.00	0.54749D-04	0.54774D+05	8.50929	0.29688	0.03013
8.00	0.54846D-04	0.54871D+05	8.51175	0.29696	0.03014
9.00	0.54895D-04	0.54919D+05	8.51346	0.29702	0.03015
10.00	0.54919D-04	0.54944D+05	8.51461	0.29705	0.03015
11.00	0.54932D-04	0.54957D+05	8.51536	0.29708	0.03016
12.00	0.54939D-04	0.54964D+05	8.51584	0.29709	0.03016

